JOURNAL OF THERMOPHYSICS AND HEAT TRANSFER
Vol. 14, No. 2, April–June 2000

Conduction and Radiation Heat Transfer in High-Porosity Fiber Thermal Insulation

Siu-Chun Lee and George R. Cunnington
Applied Sciences Laboratory, Inc., Hacienda Heights, California 91745

Nomenclature

a, b = partial wave coefficients
C = radiative cross section
F = orientation distribution function
f_v = fiber volume fraction
G_λ = asymmetry scattering factor; Eq. (23)
I_b = black-body radiation
$I_{b\lambda}$ = Planck function
i_λ = fiber-scattering intensity distribution
K_λ = extinction coefficient
k_r = radiative conductivity
k_0 = propagation constant
L = specimen thickness
M = number of fiber polar orientations
m_g = molecular mass of gas-phase material
m_s = molecular mass of solid-phase material
N = number of fiber sizes
n = real part of complex refractive index
P = size of the equivalent pore spaces inside aerogel
p_λ = scattering phase function
q = heat flux
r = radius of fiber
T = temperature
x_i = fractional volume of fibers of radius r_i
α = size parameter, $2\pi r/\lambda$
Γ_λ = modified extinction coefficient; Eq. (22)
γ = ratio of specific heats at constant pressure and constant volume
δ_s = solid fraction of matrix medium
η = scattering angle
θ = angle of observation
λ = wavelength
μ = direction cosine of angle ξ
ξ = polar angle
σ = Stefan–Boltzmann constant
σ_a = absorption coefficient
σ_s = scattering coefficient
ϕ = angle of incidence
ω = azimuthal angle

Subscripts

a = absorption
e = extinction
f = fiber
i = incident
r = random
s = scattered
λ = wavelength

Introduction

RADIATIVE transfer through fibrous media has been a subject of considerable interest for many years because of the widespread use of fiber composites as thermal insulations from cryogenic to very high temperatures. Commercially available high-porosity fiber insulations cover the range from low-cost fiber batting-type building insulations to the sophisticated and very expensive insulation composites used in aerospace thermal protection systems such as for the Space Shuttle Orbiter vehicle. The thermal effectiveness of these low-to-moderate bulk density fiber insulations arises

Siu-Chun Lee is President of Applied Sciences Laboratory, Inc., and is a thermal engineer who specializes in the design, analysis, and testing of spacecraft thermal control systems and components. He has been conducting research in radiative energy transport through fibrous media. He has published and presented over 50 papers on radiative heat transfer in high-porosity fibrous media, dependent scattering in high-density fibrous media, and spacecraft thermal control. Dr. Lee is a Senior Member of AIAA, as well as a member of the American Society of Mechanical Engineers and the Optical Society of America.

George Cunnington is a consultant and has over 30 years of experience in the development of advanced thermal control technologies and various advanced thermal insulation materials. He has authored over 90 technical papers in various areas of heat transfer and thermal control and has received three NASA technical achievement awards for thermal insulation and thermal control technologies. He was Associate Editor for the *Journal of Thermal Insulation* from 1977 to 1982. He is an Associate Fellow of AIAA and a member of the American Society of Mechanical Engineers.

Received 26 July 1999; revision received 7 December 1999; accepted for publication 10 December 1999.

from the ability of the fibers to strongly suppress radiative energy transport by scattering and absorption. The parameters that govern radiation transport are the optical properties, size, solid volume fraction, and the orientation of the fibers, as well as the optical properties of the matrix in which the fibers are dispersed.

The majority of commercial thermal insulations are high-porosity materials that typically contain less than 10% fibers by volume. The average spacing between fibers in these materials is large compared to the fiber diameter and wavelength of the incident radiation, which are the characteristic conditions of independent scattering. Thermal insulations for specialized applications, such as refractory combustion chamber liners and high-strength fiber-reinforced ceramic composites, have fiber volume fractions of 0.2 and greater. In these materials the average fiber separation is comparable to the fiber diameter and wavelength of the incident radiation. Radiation transport through high-density fiber materials involves the complex phenomena of dependent scattering, which is beyond the scope of this paper. A demarcation of the independent and dependent scattering regimes for fibrous media is given in the literature.[1]

Radiation is the primary mode of heat transfer in high-porosity fiber thermal insulations even at temperatures above a few hundred Kelvin. Consequently, many studies have reported on the modeling of radiation heat transfer through high-porosity fibrous media. The early radiation models were based on semi-empirical approaches of curve fitting with experimental data, which thus have limited applicability for analysis of insulations of different compositions. Later models applied the rigorous theoretical radiative properties of a single fiber, but the agreement with experimental data was generally poor because of the inadequate formulation to account for the composition and morphology of the fibrous medium. A review of the various radiation models is given in a recent article.[2]

In recent studies a theoretical radiation model that uses only deterministic parameters which define the composition and morphology was demonstrated to predict accurately both the radiative properties and heat-transfer characteristics of fiber insulations. These deterministic parameters include distributions of fiber size and orientation, fiber and matrix volume fractions, and the spectral complex refractive index of the fibers and matrix. An accurate theoretical model serves the multiple purposes of 1) enabling accurate thermal analyses that involve combined modes of heat transfer, 2) providing an analysis tool for evaluating the influence of material composition and morphology on the thermal performance, and 3) providing a design tool to tailor the composition of new materials to meet specific thermal performance goals.

The objective of this paper is twofold. First, we present the improved theoretical model for the prediction of radiative properties of and radiative heat transfer in high-porosity fiber thermal insulations. Second, we demonstrate the validity of the model by comparing numerical predictions with a comprehensive database of experiments, most of which were obtained by other investigators before the present model was developed. The paper begins with a brief review of the literature. The theoretical considerations of radiative properties are next described, followed by the development of the theoretical model for radiation heat transfer leading to the model for total heat transfer, including solid and gaseous conduction. Convection is neglected as the test configurations and experimental conditions preclude natural convection in the heat-transfer results.

Background

There is a large body of literature, going back over the past 50 years, devoted to the study of heat transfer in high-porosity fibrous thermal insulations. A review of the various radiation models is given in a recent article.[2] Although many researchers were also concerned with conduction through the gas and solid phases of an insulation, all addressed radiation as it is typically the dominant mode of heat transfer, even for cryogenic applications where the insulations are evacuated to prevent condensation of air.[3] Convection was negligible for the applications under consideration.

Early studies[4–15] treated radiation by developing a radiation thermal conductivity, which was either derived from curve fitting of experimental heat-transfer data or from simplified radiative transfer models. Typically, heat transfer through a specimen was measured as a function of temperature and, in some cases, air pressure. The thermal conductivity was calculated as the ratio of the measured heat flux to the temperature difference across the thickness of the specimen. This total thermal conductivity was then used with a variety of curve-fitting techniques to calculate coefficients and exponents for some assumed functional dependence of the conductivity for radiation and conduction as a function of temperature, pressure, etc. The conductivity caused by radiation was usually based on simplified radiation models that employed approximate scattering and extinction properties. This radiation conductivity, which contained fitted parameters based on experimental data, was then used in thermal analyses to extrapolate the performance of the insulation for boundary conditions other than those of the thermal conductivity test. Although these models served the important purpose of facilitating system thermal analyses, they were not adequate to guide the design of new material for improved thermal performance. This limitation is evident by the empirical nature of the radiation conductivity model, in which the fitted parameter does not contain any fundamental relationship with the actual material composition and morphology.

Later models[16–26] used the radiative properties, which include the extinction and scattering cross sections and scattered intensity distribution for an infinite cylinder based on the scattering solution of Maxwell's equations. Fibers were modeled as infinite cylinders because fibers in most commercial thermal insulations are several micrometers in diameter and a few millimeters in length. Large length-to-diameter and length-to-wavelength (in the thermal radiation regime) ratios exceeding 100 are necessary conditions for the validity of approximating a fiber as an infinite cylinder.[27] The extinction and scattering cross sections and scattered intensity distribution of fibers were formulated as a function of the fiber optical constants and diameter, as well as the wavelength. Because fibers are two-dimensional particles, their radiative properties vary with the angle of incidence. Therefore, fibers were always assumed to be randomly oriented in space so that the angular dependence of the radiative properties was removed by integrating over all incident angles. Despite the attempt to apply the rigorous formulas for an infinite cylinder, these models yielded poor agreement with measured data. This discrepancy can be attributed to the deficiency in the formulation of the radiative properties to properly account for the two-dimensional scattering characteristics of fibers in the medium.

Another theoretical approach is the inversion method to determine the fiber radiative properties using experimental data.[28–34] The phase function usually takes the form of anisotropic scattering, which is expressed in terms of several unknown parameters. The extinction and scattering coefficients are also treated as unknowns. All of the unknown parameters are varied in the solution of the radiative transfer equation to produce a best fit with measured reflectance and transmittance. This method typically involves the empirical fitting of a large number of variables, such as six constants in the study by Nicolau et al.[34] It is a formidable task to apply inverse methods to radiative heat-transfer calculations because fitting of the empirical constants must be done at each wavelength due to the usually strong variation of the radiative properties with wavelength. However, spectral inversion is seldom performed because of the extremely tedious effort required. The deficiencies of the inversion method are the uniqueness of the fitted parameters and the applicability of the fitted parameters. The uniqueness is often questionable because of the large number of variables in the inversion. The fitted parameters are not applicable to materials of different composition or properties. The benefit of inversion is that it can be applied to any scattering medium, irrespective of the nature of the scatterers because the fitted parameters have no physical correspondence with the actual material. Thus, in cases when the medium is unknown or when rigorous theoretical formulation for the properties of the medium is absent, the inversion method is the only approach that can yield an analytical model for use in radiative or heat-transfer analyses.

Formulations for the scattering properties that rigorously account for the orientation of fibers in the medium were developed

by Lee[35–38] by considering the two-dimensional scattering characteristics of fibers. The formulas for radiative properties, i.e., extinction and scattering coefficients and scattering phase function, were given as a function of the orientation, size distribution, and volume fraction of fibers. These studies revealed that fiber orientation exerts a significant effect on radiative properties. The extinction and scattering coefficients are largest for fibers oriented parallel to the boundaries, lowest if they are oriented normal to the boundaries, and intermediate for random orientation. The scattering phase function was shown to be different for random and nonrandom fiber orientations. Boulet and his coworkers[39–41] used these models to obtain good correlation of predicted and measured radiative properties of fibrous media.

Heat transfer by combined radiation and conduction in fibrous media has been addressed by many investigators using a simple additive model in terms of the thermal conductivities for radiation and conduction; the latter includes conduction through the solid lattice of the fiber medium and any gas present in the insulation. The radiative conductivity is expressed in terms of the Rosseland mean coefficient based on the diffusion approximation. The validity of this approach is dependent on the optical thickness of the insulation and the ratio of conduction to radiation.[42] Assumptions of gray behavior and isotropic scattering have been employed for many of the solution techniques.[43,44] Keller and Blumenberg[45] and Petrov[46] treated the nongray problem by an extinction coefficient and phase function spectrally weighted by the Planck distribution. Petrov compared the calculations for the transient response of silica fiber insulation exposed to an Earth reentry heating profile using both the diffusion model and the radiative thermal conductivity model in conjunction with the energy equation. These results were compared with experimental in-depth temperature measurements, and the diffusion model was shown to be more accurate for the highly transient, high heat flux conditions. The radiation conductivity based on the diffusion approximation was applied to the analysis of experimental data obtained under steady-state conditions for high-porosity fiber insulation as a function of boundary temperature and pressure of air from vacuum to atmospheric pressure.[47]

The present theoretical radiation model includes formulations for radiative properties and thermal conductivity of fibrous media. The formulations are not restricted to media that contain fibers randomly oriented in space, but are generally applicable to media with any fiber orientation. The thermal conductivity formulation accounts for the radiation conductivity from fibers, solid conduction through the fiber matrix, conduction through the gas inside the void space between fibers, and radiation absorption by the medium that contains the fibers. The model uses only deterministic parameters that define the composition and morphology of the medium. These parameters are the fiber size and orientation distributions, fiber and matrix volume fractions, and the spectral complex refractive index of the fibers and matrix. The present model does not use any assumed parameters or those obtained by fitting with experimental data.

Validation of the present theoretical model is achieved by comparison with an extensive set of radiative properties and heat-transfer data on four categories of thermal insulation materials. These are bonded and unbonded fibers, randomly oriented in free space, and unbonded fibers of both random and preferential orientation in an aerogel matrix. Aerogel is absorbing but nonscattering in the infrared spectral region. Fiber materials include alumina, silica, and silicon carbide. Much of the experimental data used for comparison were published in the literature over the past 30 years, as well as some data recently obtained by the authors.

Theory

The analysis of radiative energy transport through an absorbing and scattering medium is a classical problem that has been treated extensively in the literature. The governing equation of radiation transport is the radiative transfer equation (RTE), which is commonly given in heat-transfer textbooks. Derivation of the RTE follows from the consideration of absorption and scattering of radiative intensity along the line of sight, as well as scattering and emission of radiation into the line of sight. The general RTE is given by

$$\mu \frac{\mathrm{d}I_\lambda(\Omega)}{\mathrm{d}y} + K_\lambda(\Omega) I_\lambda(\Omega) = \sigma_{s\lambda}(\Omega) I_{b\lambda} + \frac{1}{4\pi} \int_{\Delta\Omega'} \sigma_{s\lambda}(\Omega') p_\lambda(\Omega' \rightarrow \Omega) I_\lambda(\Omega')\, \mathrm{d}\Omega' \tag{1}$$

where the variation of the radiative intensity with distance is implicit. The angular dependence of the radiative properties is explicitly highlighted in the RTE because it represents the major difference between media that contain two-dimensional scatterers such as fibers and those that contain spheres. In particular, the scattering coefficient and phase function p_λ appear inside the integral as a group because the latter characterizes the distribution of scattered intensity that arises from the scattering cross sections of the particles caused by the radiation traversing in the direction defined by the solid angle Ω'. The radiative coefficients are generally treated as angular invariant in most radiation textbooks, as the scatterers commonly encountered are spherical particles. This added complexity of angular dependent radiative properties is critical to the consideration of radiation transport through fibrous media.

Because fibers are two-dimensional scatterers, accurate calculation of radiative transport and radiation heat transfer through fibrous media requires the use of radiative properties that properly account for the orientation of fibers in the RTE. In the following subsections formulation of the radiative properties of a single fiber and then of a medium of fibers are first presented. The theoretical model for radiative and total heat transfer through fibrous media is next described. This is then followed by the validation of the theoretical model by comparison with experimental data on various types of fiber materials.

Scattering by a Single Fiber

A fiber can be modeled as an infinite cylinder if its length is large compared to its diameter and the wavelength of the incident radiation. These conditions are usually satisfied by fibers in thermal insulation materials because they are usually a few millimeters long and several micrometers in diameter. Scattering by an isolated infinite cylinder is a classical problem whose solution is well known. Details of the solution for a homogeneous cylinder may be found in Lind and Greenberg,[48] van de Hulst,[49] and Kerker.[50] The extinction and scattering cross sections per unit length for unpolarized radiation at oblique incidence on an infinite cylinder as shown in Fig. 1 are given by

$$C_{e\lambda}(\phi) = \frac{2}{k_0} Re \sum_{n=-\infty}^{\infty} (b_n^I + a_n^{II}) \tag{2}$$

$$C_{s\lambda}(\phi) = \frac{4}{k_0} \left[\frac{1}{2} \left(\left| b_0^I \right|^2 + \left| a_0^{II} \right|^2 \right) + \sum_{n=1}^{\infty} \left(\left| b_n^I \right|^2 + \left| a_n^{II} \right|^2 + 2 \left| a_n^I \right|^2 \right) \right] \tag{3}$$

respectively, where a_n and b_n are partial wave coefficients that are functions of the fiber material refractive index and the superscripts I and II refer to the transverse magnetic and transverse electric mode, respectively. The corresponding solutions for a radially stratified cylinder have been given by Barabas.[51] The scattered intensity distribution from the cylinder is given by

$$i_\lambda(\theta, \phi) = \frac{1}{2} \left[\left| b_0^I + 2 \sum_{n=1}^{\infty} b_n^I \cos(n\theta) \right|^2 + 2 \left| \sum_{n=1}^{\infty} a_n^I \sin(n\theta) \right|^2 + \left| a_0^{II} + 2 \sum_{n=1}^{\infty} a_n^{II} \cos(n\theta) \right|^2 \right] \tag{4}$$

Note that ϕ is the polar angle measured from the normal to the axis of the cylinder, whereas θ is the azimuthal angle measured

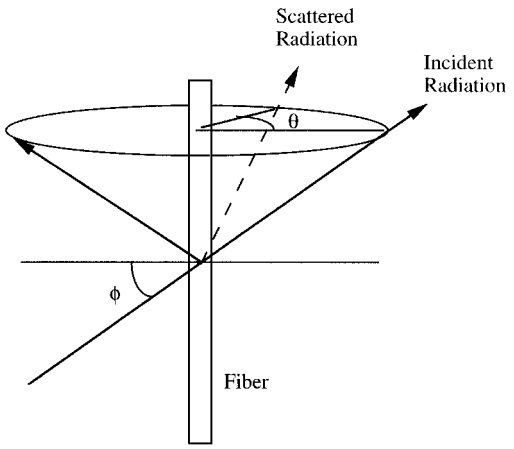

Fig. 1 Scattering geometry for a single cylindrical fiber.

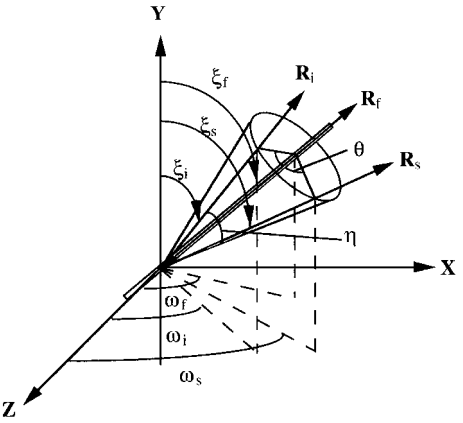

Fig. 2 Scattering geometry for an oriented fiber relative to a reference frame.

on the plane normal to the cylinder axis. Both the radiative cross sections and scattered intensity distribution vary with the angle of incidence ϕ.

Radiative Properties of Fibrous Media

Although scattering by a single fiber is specified with respect to the cylindrical polar coordinate system centered on the longitudinal axis of the fiber (cf. Fig. 1), scattering by an oriented fiber in a medium of fibers must be prescribed relative to the global coordinate system as shown in Fig. 2 in order to properly account for the effect of each fiber. Therefore, transformation of fiber radiative properties from a fiber-centered to the global coordinate system is essential to the correct analysis of the radiative properties of fiber materials.

The transformation between the scattering angles relative to the two coordinate systems can be derived rigorously from geometric considerations. Denoting the directions of the fiber axis and the incident and scattered radiation by the polar angle ξ and azimuthal angle ω in the global coordinate system, the relations between the fiber-centered and global coordinate systems are given by[35]

$$\cos\eta = \sin\xi_i \sin\xi_s \cos(\omega_i - \omega_s) + \cos\xi_i \cos\xi_s \tag{5}$$

$$\cos\eta = \cos\theta\cos^2\phi + \sin^2\phi \tag{6}$$

$$\sin\xi_i \sin\xi_f \cos(\omega_i - \omega_f) + \cos\xi_i \cos\xi_f = \sin\xi_s \sin\xi_f \cos(\omega_s - \omega_f) + \cos\xi_s \cos\xi_f \tag{7}$$

where η is the angle between the propagating directions of the incident and scattered radiation. Equation (6) gives the relationship between the fiber-centered coordinates (θ, ϕ) and η defined in the global coordinate system. The maximum value of η for a given set of incident and fiber direction follows from Eq. (6) as the apex angle $\pi - 2\phi$ of the scattering cone. In a fiber medium the orientation of each fiber is different, thereby resulting in a different scattering cone for each fiber. The constraint on the incident and scattering directions for a given fiber orientation is given by Eq. (7).

The spectral extinction and scattering coefficients of a fiber medium are obtained by weighting the respective radiative cross sections over the distributions of fiber size and orientation as[35]

$$\{K_\lambda, \sigma_{s\lambda}\}(\xi_i, \omega_i) = \int_0^{2\pi}\int_0^{\pi/2}\int_{r_1}^{r_2} \{C_{e\lambda}(\phi), C_{s\lambda}(\phi)\} N[r(\xi_f, \omega_f)] \times F(\xi_f, \omega_f)\, dr\, d\xi_f\, d\omega_f \tag{8}$$

where $N(r)\,dr$ specifies the number of fibers with radius between r and $r + dr$ that are oriented in the direction (ξ_f, ω_f) as prescribed by the orientation distribution function $F\,d\xi_f\,d\omega_f$. The radiative coefficients are per unit length because the fibers are infinitely long compared to the wavelength. The radiative coefficients are generally a function of the incident direction (ξ_i, ω_i).

Formulation of the scattering phase function for a fiber medium requires careful consideration of the two-dimensional scattering behavior of fibers. This contrasts with the one-dimensional scattering behavior of spheres whose scattering cross section and scattered intensity distribution are independent of incident radiation direction. The phase function for a medium of spheres is then identical to that for a single sphere. Because the scattering cross section of a fiber varies with incident angle, the scattered intensity distribution also varies with incident direction. The product of the single-fiber cross section and intensity distribution must be treated as a single scattering function[38]:

$$C_{s\lambda} p_\lambda(\theta, \phi) = \frac{4\lambda}{\pi^2} \frac{i_\lambda(\theta, \phi)}{\sin\theta\cos^2\phi} \tag{9}$$

This function denotes the distribution of scattered intensity corresponding to the scattering cross section $C_{s\lambda}$ at the incident angle ϕ, and integration of $C_{s\lambda} p_\lambda$ over all θ yields $C_{s\lambda}$. Because the orientation of each fiber is different in a fibrous medium, the phase function of a medium of fibers is generally different from that of a single fiber. The product of scattering coefficient and phase function for a fiber medium is obtained by integrating $C_{s\lambda} p_\lambda(\theta, \phi)$ for a single fiber over the size and orientation distribution functions[38]:

$$\langle \sigma_{s\lambda} P_\lambda \rangle(\eta; \xi_i, \omega_i) = \int_0^{2\pi}\int_0^{\pi/2}\int_{r_1}^{r_2} C_{s\lambda} p_\lambda N[r(\xi_f, \omega_f)] \times F(\xi_f, \omega_f)\, dr\, d\xi_f\, d\omega_f \tag{10}$$

where the dependence on incident direction is shown explicitly. The variation of the scattered intensity distribution with incident angle is a consequence of the directional dependence of the scattering coefficient.

Equations (8) and (10) are the governing relations from which the radiative properties of fiber materials with any size and orientation distribution can be obtained. In most fiber materials no correlation exists between the fiber orientation and size distribution, and the latter usually consists of a discrete number of fiber radii. Also, fibers are oriented either randomly in space or in predominant polar directions ξ_f but random in the azimuth ω_f or in a combination of random and preferential orientations. Radiative properties formulas for these fiber orientations are given explicitly here because material types with these fiber orientations are used in the experimental validation of the theoretical radiation model.

Medium of Fibers Oriented Randomly in Space

The spectral extinction and scattering coefficients for fibers oriented randomly in space with a discrete distribution of fiber sizes are given by[38]

$$\{K_{\lambda r}, \sigma_{s\lambda r}\} = \frac{f_v}{\pi} \sum_{j=1}^{N} \frac{x_j}{r_j^2} \int_0^{\pi/2} \{C_{e\lambda}(\phi), C_{s\lambda}(\phi)\} \cos\phi\, d\phi \tag{11}$$

where x_j is the fraction of fibers of radius r_j. The product of scattering cross section and phase function is given by[38]

$$\langle \sigma_{s\lambda r}\, p_{\lambda r}\rangle(\eta) = \frac{4 f_v \lambda}{\pi^3} \sum_{j=1}^{N} \frac{x_j}{r_j^2} \times \int_0^1 \frac{i_\lambda(\eta, \phi)}{\sqrt{(1-\cos\eta)(1+\cos\eta-2\sin^2\phi)}}\, \mathrm{d}(\sin\phi) \tag{12}$$

Equations (11) and (12) indicate that the radiative properties of a medium of fibers randomly oriented in space are independent of incident direction.

Medium of Fibers in Preferential Polar Orientations

The extinction and scattering coefficients of a fiber medium containing fibers inclined at multiple polar directions ξ_{fk} but randomly oriented in the azimuth ω_f are given by[38]

$$\{K_\lambda, \sigma_{s\lambda}\}(\xi_i) = \frac{f_v}{\pi^2} \sum_{k=1}^{M} y_k \sum_{j=1}^{N} \frac{x_j}{r_j^2} \times \int_0^\pi \{C_{e\lambda}(\phi), C_{s\lambda}(\phi)\}\delta(\xi_f - \xi_{fk})\, \mathrm{d}\omega_f \tag{13}$$

where y_k is the fraction of fibers inclined at ξ_{fk} and δ is the delta function. The product of the scattering coefficient and phase function is given by[38]

$$\langle \sigma_{s\lambda}\, p_\lambda\rangle(\eta; \xi_i) = \frac{4 f_v \lambda}{\pi^4} \sum_{k=1}^{M} y_k \sum_{j=1}^{N} \frac{x_j}{r_j^2} \times \int_{\sin\phi_-}^{\sin\phi_+} \int_0^{\pi/2} F\delta(\xi_f - \xi_{fk})\, \mathrm{d}\xi_f\, \mathrm{d}(\sin\phi) \tag{14}$$

where

$$F = \frac{i_\lambda(\eta, \phi)/\sqrt{(1-\cos\eta)(1+\cos\eta-2\sin^2\phi)}}{\sqrt{(\sin\phi_+ - \sin\phi)(\sin\phi - \sin\phi_-)}} \tag{15}$$

$$\sin\phi_\pm = \cos\xi_i \cos\xi_{fk} \pm \sin\xi_i \sin\xi_{fk} \tag{16}$$

Equations (13) and (14) show that the radiative properties of fiber media containing preferentially oriented fibers in the polar direction but random in the azimuth are a function of only the polar incident angle.

Mixture of Fibers in Mixed Random and Aligned Orientations

For media that contain a mixture of fibers oriented in spatially random and in several polar directions, the radiative properties are computed as a weighted sum of all of the fiber orientations. The radiative coefficients and scattering phase function are given by[52]

$$\{K_\lambda, \sigma_{s\lambda}\}(\xi_i) = y_r\{K_{\lambda r}, \sigma_{s\lambda r}\} + \sum_{k=1}^{M} y_k\{K_\lambda(\xi_i, \xi_{fk}), \sigma_{s\lambda}(\xi_i, \xi_{fk})\} \tag{17}$$

$$\langle \sigma_{s\lambda}\, p_\lambda\rangle(\eta; \xi_i) = y_r\langle \sigma_{s\lambda r}\, p_{\lambda r}\rangle(\eta) + \sum_{k=1}^{M} y_k\langle \sigma_{s\lambda}\, p_\lambda\rangle(\eta; \xi_i, \xi_{fk}) \tag{18}$$

and

$$y_r + \sum_{k=1}^{M} y_k = 1 \tag{19}$$

is the conservation equation.

Radiation Heat Transfer

High-porosity fiber insulation materials are optically thick because their extinction coefficient is generally of the order of 10^2/cm and the insulation thickness is typically greater than 1 cm. The diffusion approximation, which is discussed in standard radiation texts,[42] can be used to describe radiation heat transfer. The classic diffusion model commonly used for optically thick, nonscattering media is modified to account for the effect of scattering by fibers and absorption by the matrix medium. Within the context of the diffusion approximation, radiation heat transfer can be treated similar to the Fourier law of heat conduction in terms of a radiative conductivity k_r:

$$q_r = -k_r \frac{\mathrm{d}T}{\mathrm{d}y} \tag{20}$$

The radiative conductivity is conventionally calculated by using the Rosseland mean absorption coefficient, which involves the absorption coefficient $\sigma_{a\lambda}$ of the nonscattering matrix medium:

$$k_r = \frac{16\sigma T^3}{3} \int_0^\infty \frac{1}{\sigma_{a\lambda}} \frac{\mathrm{d}I_{b\lambda}(T)}{\mathrm{d}I_b(T)}\, \mathrm{d}\lambda \tag{21}$$

To account for the presence of fibers and their two-dimensional scattering characteristics, $\sigma_{a\lambda}$ is replaced by the modified absorption coefficient Γ_λ, which is defined as[52–54]

$$\Gamma_\lambda = K_\lambda(\mu_0)(1 - G_\lambda) + \sigma_{a\lambda} \tag{22}$$

where $K_\lambda(\mu_0)$ is the extinction coefficient of the fiber medium evaluated in the heat flow direction μ_0 (=cos ξ_0) and G_λ is the asymmetry scattering factor. The coefficient $\sigma_{a\lambda}$ is a property of the matrix medium, which must be either measured using a matrix specimen without fibers or estimated based on the physical properties and composition of the matrix. The scattering factor G_λ represents the total scattered radiation caused by incident radiation traversing in the heat flow direction. It is given by[52–54]

$$G_\lambda = \frac{1}{K_\lambda(\mu_0)} \int_0^1 \int_{-1}^1 \langle \sigma_{s\lambda}\, p_\lambda\rangle(\mu_i, \mu_s)\mu_i\, \mathrm{d}\mu_i\, \mathrm{d}\mu_s \tag{23}$$

where

$$\langle \sigma_{s\lambda}\, p_\lambda\rangle(\mu_i, \mu_s) = \frac{1}{2\pi} \int_0^{2\pi} \langle \sigma_{s\lambda}\, p_\lambda\rangle(\eta; \xi_i)\, \mathrm{d}\omega_i \tag{24}$$

is the scattering coefficient-phase function product for media containing fibers randomly oriented in the azimuthal direction. Note that $\langle \sigma_{s\lambda}\, p_\lambda\rangle(\eta; \xi_i)$ is given by Eq. (12) for spatially randomly oriented fibers, Eq. (14) for fibers with preferential polar orientations, and Eq. (18) for fibers in a mixture of random and preferential orientations. Scaling of K_λ by $(1 - G_\lambda)$ yields an absorption coefficient that is consistent with the inherent assumption of the diffusion approximation.

Conduction Heat Transfer

Although the dominant mode of heat transfer through high-porosity fiber thermal insulations is generally radiation, the contributions of conduction through the solid phase, i.e., fibers, and any gas present in the void space between the fibers must be accounted for when comparing theoretical predictions with measured heat-transfer data. In some applications where the temperature difference, dimension, and/or insulation permeability are large, convection can become a major contributor to the total heat transfer. Many studies have addressed this problem.[55] However, convection is not a consideration for the experimental heat-transfer data used in the present study. Heat-transfer measurements were made either in vacuum or in air using a horizontal slab geometry with a small vertical dimension of typically 2.54 cm, and the temperature difference across the slab is nominally 100 K.

Solid-phase conduction is strongly dependent on the type of fiber lattice and the matrix material in which the fibers are embedded. It consists of a very complex combination of multiple series-parallel

paths along fibers, across fiber-to-fiber contacts, and from fiber-to-matrix contacts. Gas-phase conduction is a more tractable problem, its solution being related to the Knudsen number based upon the mean free path of the gas at a given temperature and pressure and the mean size of the pores making up the void space. Because the characteristics of solid and gas conduction are strongly dependent on the material structure, the following subsections describe the analytical approaches employed to evaluate solid and gas conduction effects in the different types of fiber materials for which their data are used in the present study. These materials include self-supporting insulations that contain bonded fibers and unbonded fibers and unbonded fibers in an absorbing matrix. Heat-transfer measurements were conducted in vacuum for the former materials and in air at atmospheric pressure for the latter.

Conduction Through Solid Phase of Bonded Fibers

An example of bonded fibers in a free space matrix is the LI900 Space Shuttle Orbiter thermal protection tile materials,[14] whose data are being used in the present study. LI900 consists of a rigid structure of bonded silica fibers, which is formed by sintering at high temperatures (cf. Fig. 3). An exact theoretical treatment of solid conduction for this complex geometry presents a formidable problem because of the tenuous nature of the myriad of different paths of varying fiber lengths and cross-sectional areas, as well as the unknown conductances through the bonded fiber-to-fiber contacts.

The solid-phase thermal conductivity k_c of LI900 materials is calculated by using a semi-empirical approach based on the global thermal resistance concept. It is written in terms of the bulk density of the fiber matrix ρ_s and the thermal conductivity of the fiber material k_s as[54]

$$k_c(T) = F_s \rho_s k_s(T) \tag{25}$$

where the temperature dependence is shown explicitly. The parameter F_s is a global property that relates the microscale geometric effects of the fiber matrix with bulk dimensions. It accounts for the various fiber path lengths, series-parallel arrangement of fibers in the matrix, and dimensions of fiber-to-fiber contacts. It is, therefore, unique for each fiber material and must be determined from measurement. Because thermal expansion effects are generally negligible for silica fibers, F_s may be treated as independent of temperature, and it can be determined from heat-transfer measurements on the fiber material in vacuum at cryogenic temperature. Under these conditions radiation is negligible and gas conduction is nonexistent, so that solid conduction is the only significant mode of heat transfer. The measured heat flux and boundary temperatures yield k_c, and F_s follows from Eq. (25) by using the known material properties ρ_s and k_s at the mean temperature of the boundaries.

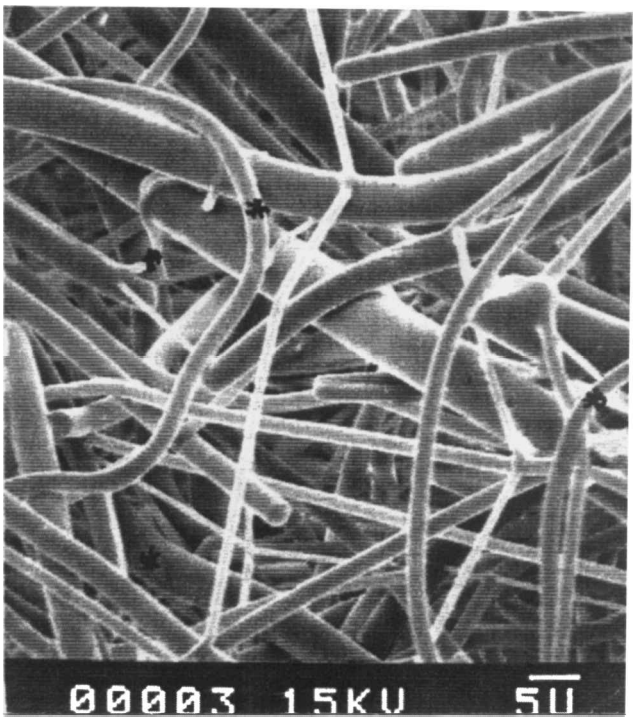

Fig. 3 SEM of bonded fibers; magnification = 1200X.

Conduction Through Solid Phase of Unbonded Fibers

High-porosity, loose fiber batts such as those used in building insulations contain unbonded fibers. These fiber materials are commonly used under atmospheric conditions so that air permeates throughout the voids inside the fiber matrix. The semi-empirical approach used to treat the thermal conductivity of bonded fibers is used in the case of unbonded fiber insulation. The solid-phase thermal conductivity of an unbonded fiber matrix is assumed to take a similar form as Eq. (25), except that the presence of gas in the void space affects this solid conductance in a nonlinear manner. Thus, the solid-phase thermal conductivity may not be treated as independent of gas species, temperature, and pressure. For high-porosity fibrous insulations the solid conductivity is independent of fiber diameter and varies with density raised to a power as[3,10,14]

$$k_c(T) = F_s \rho_s^b k_s(T) \tag{26}$$

where $1 \leq b \leq 2$. The geometric parameter F_s is also determined from experimental data in vacuum at cryogenic temperature. This thermal conductivity is much smaller for unbonded fibers as the fiber-to-fiber contact conductance is orders of magnitude smaller than that for bonded fibers.

Conduction Through Solid Phase of Fiber-Loaded Aerogels

Another type of fiber insulation is a fiber-reinforced composite in which fibers are dispersed in a continuous purely absorbing matrix. An example of this is the fiber-loaded aerogel in which fibers are distributed in a low-density aerogel matrix. For thermal insulation applications the fiber volume fraction is typically less than 0.06, and the aerogel solid fraction is less than 0.05. The aerogel matrix suppresses gaseous conduction, and the fibers reduce radiation while enhancing the strength of the intrinsically weak aerogel.

Aerogel, first developed by Kistler[56] nearly 70 years ago, is an open-cell, transparent material in which 90% of the pores range in size from 10 to 50 nm (Refs. 57 and 58). The small pores suppress convection and gaseous conduction in nonevacuated applications, and the resultant thermal conductivity for the solid and gas phases is on the order of 10^{-2} W/m-K (Ref. 59). Because silica aerogels are transparent to infrared radiation, they are undesirable as a thermal insulation even at moderate temperatures, despite their very low solid- and gas-phase thermal conductivity. Addition of absorbing material such as pigment grade carbon black or iron compounds to the transparent aerogels have been used to effectively suppress thermal radiation.[57–59] Monolithic carbon aerogels, which are strongly absorbing, have also been produced.[60] Fibers, however, reduce radiation transport while enhancing the strength of aerogel.

Fiber-loaded aerogels are composites that contain unbonded fibers in an absorbing matrix medium. Microscopy and absorption analyses show that the skeletal structure of aerogel is made up of interlocking long chains of loosely bonded macromolecules.[57,58] Nearly 90% of the pore volume formed by these macromolecular chains consists of micropores having characteristic diameters on the order of 5–50 nm, depending on the aerogel bulk density. Solid conduction by fibers in fiber-loaded aerogels is negligible because the fibers are principally noncontacting in the aerogel matrix as shown by the scanning electron micrograph (SEM) of a fiber-loaded aerogel specimen in Fig. 4. An exact theoretical treatment of the macromolecule solid lattice conductivity is again a formidable task because of the extremely complex geometric arrays of macromolecules, as well as uncertainties in bonding strength and phonon transport within and across the bond and contact regions at a nanoscale level. Attempts to model the transport process in terms of packing arrangements of spheres[61] and with measurements of sound velocity[57] have met with limited success.

Fig. 4 SEMs of fiber-filled aerogel; magnification = 100X.

In the present study we express the solid thermal conductivity of fiber-filled aerogels by means of an empirical expression in terms of the thermal properties of the unloaded aerogel. The thermal conductivity is written similar to Eq. (26) for unbonded fibers as[52]

$$k_c(T) = A\rho_a^b k_s(T) \tag{27}$$

where A is a geometric factor that accounts for the chain-like aerogel structure and the diameter of the macromolecules, ρ_a is the bulk density of aerogel, and k_s is the thermal conductivity of the material from which the aerogel is made. The density raised to power b is a proportionality factor that accounts for the series/parallel conduction paths for a given density of aerogel without fibers. Both A and b are determined from experimental data on unloaded aerogels. For aerogel densities between 50 and 220 kg/m^3, b is estimated to vary from 1.25 to 1.5 based on experimental data on various aerogels in vacuum at low temperatures.[57,60,62,63] The aerogel conductivity is typically between 0.005 and 0.015 W/m-K at ambient temperature for bulk densities between 50 and 100 kg/m^3 and macromolecule diameters from 2 to 5 nm (Ref. 64). The higher thermal conductivity is caused by the greater bulk density, which results in a higher solid fraction and increased number of conduction paths. The thermal conductivity of unloaded aerogel is assumed to be independent of the embedded fibers for fiber volume fraction < 0.1, as the small amount of fibers would not change the solid conduction paths of the matrix medium.

Gas-Phase Conduction

The thermal conductivity caused by gas in the void space of a high-porosity fiber insulation is a function of the size of the pores that make up the void space and the mean free path of the gas. It may be expressed in terms of a modified Knudsen parameter as[3]

$$k_g(T, p) = \frac{k_{g0}(T)}{1 + 2\beta l_m / P} \tag{28}$$

where $k_{g0}(T)$ is the pressure-independent thermal conductivity of the gas, l_m is the mean free path of the gas at temperature T and pressure p, and P is the mean diameter of the pores. The parameter β is defined as

$$\beta = [2\varepsilon/(\gamma - 1)][(2 - \alpha)/\alpha] \tag{29}$$

where

$$\varepsilon = (9\gamma - 5)/4 \tag{30}$$

$$\alpha = \frac{4m_g m_s}{(m_g + m_s)^2} \tag{31}$$

In the preceding equations γ is the ratio of the specific heats at constant pressure and constant volume, and m_g and m_s are the molecular weights of gas and solid phases, respectively. The mean pore diameter for a matrix medium containing fibers randomly oriented in space is[64]

$$P = 0.524 d_p / \delta_s \tag{32}$$

and that for fibers randomly oriented in planes is

$$P = 0.785 d_p / \delta_s \tag{33}$$

where d_p is the diameter of the macromolecules that form the matrix and δ_s is the solid fraction of the matrix. For aerogel where d_p is between 2–5 nm, the thermal conductivity of air in the aerogel matrix is of the order of 10^{-2} W/m-K.

Total Heat Transfer

The total heat transfer through a fiber medium without convection includes radiation and conduction from both the gas and solid phases. By using the diffusion approximation and the radiative conductivity derived in the preceding section, the energy equation for heat transfer by combined radiation and conduction may be written as

$$\frac{\mathrm{d}}{\mathrm{d}y}\left[(k_r + k_c)\frac{\mathrm{d}T}{\mathrm{d}y}\right] = 0 \tag{34}$$

The total heat transfer through a fiber matrix of thickness L between two boundaries with emittance ε_1 and ε_2 at temperatures T_1 and T_2 is[65]

$$q_t = (1/C_0)\left\{\sigma(T_1^4 - T_2^4) + (3k_c\tau_0/4L)(T_1 - T_2)\right\} \tag{35}$$

where

$$C_0 = \frac{3\tau_0}{4} + \left(\frac{1}{\varepsilon_1} - \frac{1}{2}\right)\left[\frac{1}{1 + k_c/k_r(T_1)}\right] + \left(\frac{1}{\varepsilon_2} - \frac{1}{2}\right)\left[\frac{1}{1 + k_c/k_r(T_2)}\right] \tag{36}$$

$\tau_0 = \Gamma_0 L$ is the optical depth and Γ_0 is the total extinction coefficient that includes contributions from the fibers and the matrix medium. The total extinction coefficient is calculated similar to the Rosseland mean absorption coefficient as

$$\frac{1}{\Gamma_0} = \int_0^\infty \frac{1}{\Gamma_\lambda}\frac{\mathrm{d}I_{b\lambda}(T)}{\mathrm{d}I_b(T)}\,\mathrm{d}\lambda \tag{37}$$

where Γ_λ is the modified spectral absorption coefficient given by Eq. (22).

An effective total thermal conductivity can be defined based on the total heat flux given by Eq. (35) and the temperature gradient across the thickness of the specimen as

$$k_e = q_t L/(T_1 - T_2) \tag{38}$$

In the limit of large optical thickness, Eq. (35) reduces to

$$k_e = k_r + k_c \tag{39}$$

indicating that heat transfer by radiation and conduction are additive for optically thick media.

Table 1 Summary of test specimen characteristics

Fiber category	Material designation	Measured property	Original reference	Material	Fiber mean diameter, μm	Fiber size distribution
Bonded fibers	1.7A (A1)[a]	Radiative and heat flux	66	Fused silica	1.7	Ref. 66
	1.7B (B1)		14		1.7	
	4.0B (B2.3)				4.0	
Unbonded fibers	Silica fiber batt	Heat flux	10	Fused silica	1.3	Not given
	Silicate glass	Heat flux	20	Silicate glass	6.9	Ref. 72
Fiber-filled silica aerogel	Silica fiber	Radiative and heat flux	67	Silica	2.38	Ref. 67
	SiC fiber	Radiative and heat flux	52	SiC	15	Ref. 67
	Alumina fiber	Radiative	67	Alumina	3.3	Not given

[a]Originally designated as A1, B1, and B2.3 in Ref. 66.

Experimental Validation of Model

Two types of experiment data are used to test the theoretical model: measurements of spectral transmittance and reflectance and heat-transfer data as a function of boundary temperatures. The database includes both recent measurements and those reported in the literature over the last 30 years. The test specimens include shuttle tile materials, loose fiber batts, and fiber-filled aerogels. The fiber materials include silica, alumina, and silicon carbide, with fiber ranging from slightly over 1 μm to about 15 μm in diameter. The test specimen types, fiber properties, and the type of test are summarized in Table 1. References to the original experimental data sources are also given for each fiber category.

Radiative Properties

Validation of the theoretical formalisms for the radiative properties of fibrous media is based upon comparisons of the calculated spectral reflectance and transmittance with a large set of experimental data obtained by the authors and reported in the literature on bonded fiber thermal protection materials[66] and fiber-filled aerogel insulations.[67] The former type contains fibers bonded by sintering at fiber crossing points, and the latter contains unbonded fibers in an absorbing matrix. These materials were selected because their structural integrity is good, and the arrangement of the fibers in the test specimen is not altered by handling during either the radiative properties or the physical characterization measurements. High-porosity, loose batt fiber materials were not included in the measurement sequence because of the large uncertainties in specimen characterization caused by the poor stability of the morphology of the media. Transmittance and reflectance measurements involved the illumination of a test specimen by a collimated light source. The experimental apparatus and procedures for the radiative properties experiments have been described in detail in Ref. 66.

Prediction of spectral hemispherical reflectance and normal transmittance is based on the solution of the RTE by using the radiative properties given by Eqs. (10–19). Because measurements were made in room temperature, the RTE neglecting emission is solved for the condition of collimated incidence:

$$\mu \frac{\mathrm{d}I_\lambda}{\mathrm{d}y} + K_{m\lambda} I_\lambda = \frac{1}{2} \int_{-1}^{1} \sigma_{s\lambda} p_\lambda(\mu', \mu) I_\lambda(\mu')\, \mathrm{d}\mu' \qquad (40)$$

where the spectral extinction coefficient of the medium

$$K_{m\lambda} = K_\lambda + \sigma_{a\lambda} \qquad (41)$$

is equal to the sum of the fiber extinction coefficient K_λ and the absorption coefficient of the matrix medium $\sigma_{a\lambda}$. The boundary condition for incident intensity I_0 is

$$I_\lambda(y=0) = I_0\, \delta(\omega)\delta(\mu - 1) \qquad (42)$$

where δ is the delta function. The RTE is solved by the method of discrete ordinates using a 40-point Gaussian quadrature. Several computations were made using a 48-point quadrature, and the results showed an insignificant difference from results based on the 40-point quadrature.

The angular distributions of the transmitted and reflected intensities are obtained, and the hemispherical reflectance is given by

$$R_{h\lambda} = \pi \int_{-1}^{0} I_\lambda(\mu, y=0)\mu\, \mathrm{d}\mu / I_0 \qquad (43)$$

and the normal transmittance is

$$T_{n\lambda} = \pi \int_{\Delta\Omega} I_\lambda(\mu, y=L)\, \mathrm{d}\Omega / I_0 \qquad (44)$$

where $\Delta\Omega$ is the solid angle subtended by the detection system.

Bonded Fiber Material

Three variations of the silica fiber thermal protection insulation materials[66] were used in the validation of the theoretical models. These materials, designated as types 1.7A, 1.7B, and 4.0B, vary in fiber size distribution and volume fraction. Average fiber diameters and the standard deviations, respectively, are 1.7 and 1.26 μm for type 1.7A, 1.7 and 0.86 μm for type 1.7B, and 4.0 and 1.5 μm for type 4.0B. Fiber size distribution data for each material are given in Ref. 66. These materials were selected because their composition and morphology had previously been thoroughly characterized.[14] Figure 3 shows the physical arrangement of the fibers and the nature of the bonds at fiber crossings. Fiber orientation, as determined by microscopy, is random in space for each material. Crystallographic studies using x-ray diffraction showed that the fibers were amorphous and that no crystalline phase was formed during high-temperature material processing or testing environments. The letters A and B designate the two sources of very high purity silica raw fibers (>99.5% SiO_2) from which the insulations were produced in the period from 1973 to 1980. The reflectance and transmittance measurements used for the present comparison with theory were also made during the same time period. Accurate heat-transfer data for these materials had been reported in the original reference.[14] Consequently, theoretical predictions both of radiative properties and radiation heat transfer could be compared with experimental data from the same set of materials.

Comparisons between predicted and measured hemispherical spectral reflectance for type 1.7A, 1.7B, and 4.0B fiber materials are shown in Figs. 5–7. The maximum experimental uncertainties are 0.01 for the absolute value of reflectance and 0.01 for wavelength. Initially, the complex refractive index ($n - ik$) data of high-purity bulk-fused silica reported in the literature[68] were used in the calculation of the radiative properties and the consequent prediction of the normal spectral transmittance and hemispherical spectral reflectance of type 4.0B specimens. These predicted reflectance values, which are denoted by the solid curve in Fig. 5, generally compare well with measured data, except for the wavelength regions from 2.5 to 4.5 μm and 5.25 to 6.25 μm. The good agreement over a wide spectral range suggested that the theoretical formalism for the radiative properties is accurate. The lower reflectance in the two bands can be attributed to the presence of a surface layer more strongly absorbing than that of the bulk material. This layer may be caused by contamination, nonstoichiometry of the metal-oxygen composition at the surface, introduction of surface defects during processing, or a combination

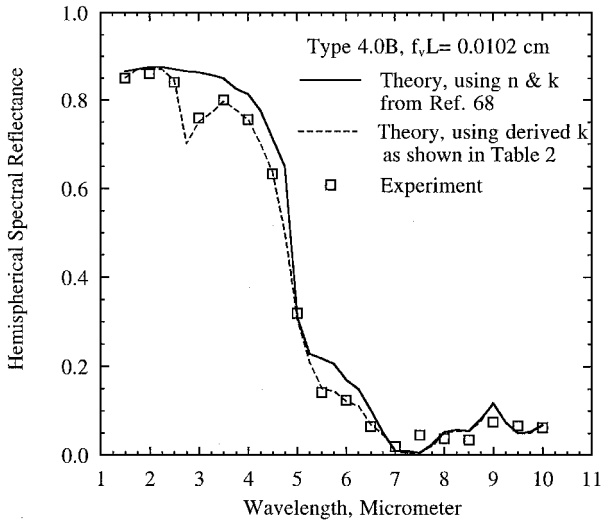

Fig. 5 Comparison of theoretical prediction based on two different sets of absorption index k with measured hemispherical spectral reflectance of type 4.0B material; f_v = 0.0677 (Ref. 66).

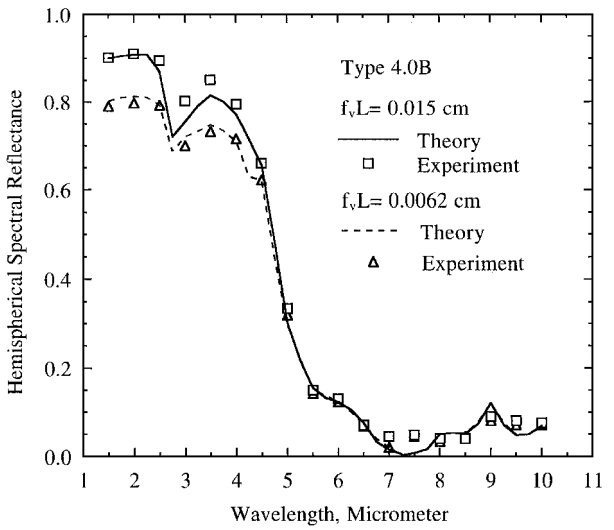

Fig. 6 Comparison of predicted and measured hemispherical spectral reflectance for two thicknesses (L) of type 4.0B material; f_v = 0.0677 (Ref. 66).

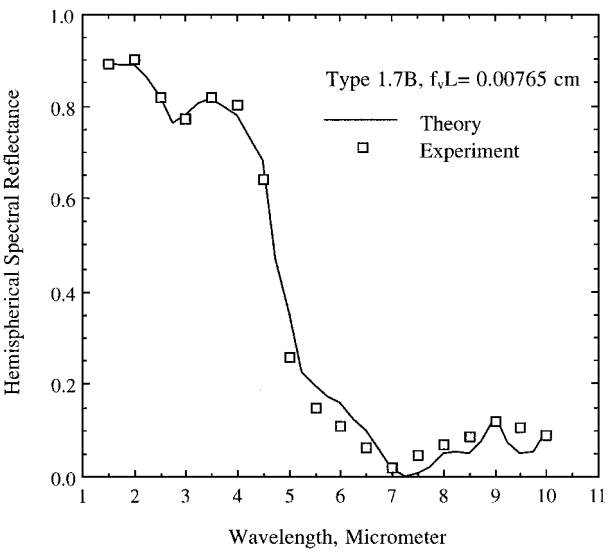

Fig. 7 Comparison of predicted and measured hemispherical spectral reflectance for type 1.7B material; f_v = 0.0736 (Ref. 66).

Table 2 Imaginary part of fiber refractive index k

Wavelength, μm	k	
	Ref. 68	Derived
2.50	4.70e−6	3.29e−5
2.75	4.70e−6	2.90e−4
3.00	1.00e−5	2.00e−4
3.25	1.00e−5	1.50e−4
3.50	1.00e−5	1.00e−4
3.75	4.00e−5	1.35e−4
4.00	6.00e−5	1.74e−4
4.25	1.30e−4	3.05e−4
4.50	2.60e−4	5.20e−4
4.75	4.80e−4	1.50e−3
5.00	3.98e−3	3.98e−3
5.25	5.77e−3	6.00e−3
5.50	5.67e−3	9.07e−3
5.75	5.82e−3	9.12e−3
6.00	6.19e−3	9.16e−3
6.50	6.70e−3	9.38e−3

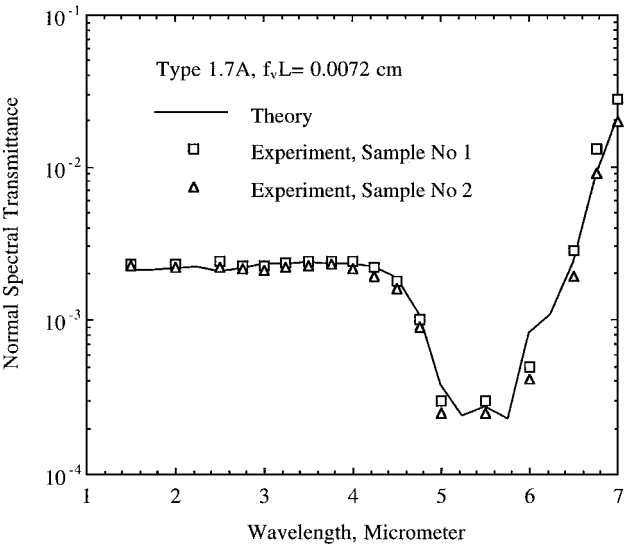

Fig. 8 Comparison of predicted and measured normal spectral transmittance for two type 1.7A equal-thicknesses (L) specimens; f_v = 0.0736 (Ref. 66).

of all. To account for the deviation of the fiber material from high-purity silica, the absorption index k between 2.5 and 6.5 μm was adjusted to minimize the difference between the predicted and measured reflectance. The values of the adjusted k and the literature data are summarized in Table 2. New predictions based on the adjusted k are shown by the dashed curve of Fig. 5. These adjusted ks were then used for all subsequent predictions for type B fiber specimens. Figure 6 shows the comparisons between theoretical and measured reflectance for two additional type 4.0B specimens with thicknesses greater and less than that of the specimen of Fig. 5. The adjusted k values were used to calculate the predictions, and the agreement is excellent over the entire spectral range. The agreement is generally within 10%. Similarly, good agreement is observed for the material made from the type 1.7B fibers, as shown in Fig. 7.

Comparisons between predicted and measured normal spectral transmittance are shown in Figs. 8–10 for type 1.7A, 1.7B, and 4.0B fiber media. The maximum uncertainty in the absolute value of transmittance is 0.0003, and it is 0.01 in wavelength. Figure 8 shows the measured data for two specimens of type 1.7A fiber insulation. The high degree of repeatability of experimental data for multiple type 1.7A specimens is evident in the figure. The type A fiber does not exhibit the strong absorption characteristics of the type B fibers as revealed by the experimental data. Hence the literature values of n and k were used in the calculation of the type A

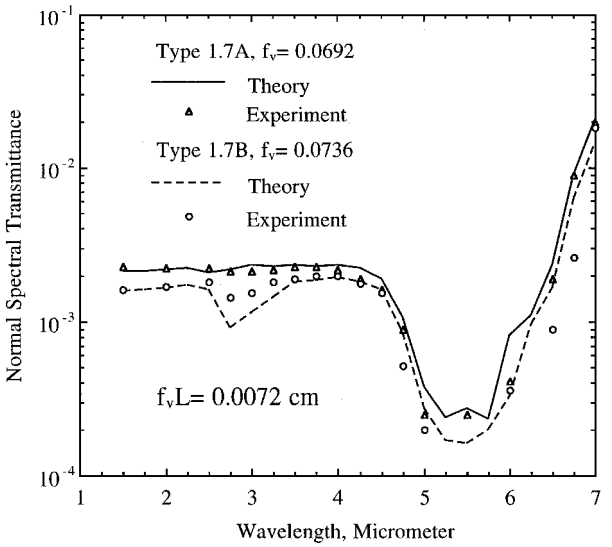

Fig. 9 Comparison of predicted and measured normal spectral transmittance for type 1.7A and 1.7B materials with identical values of f_vL = 0.0072 cm; L = specimen thickness.[66]

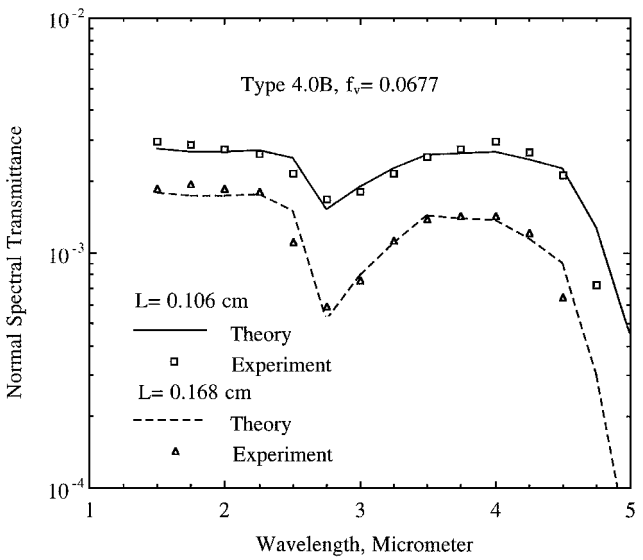

Fig. 10 Comparison of predicted and measured normal spectral transmittance for two thicknesses of type 4.0B material.[66]

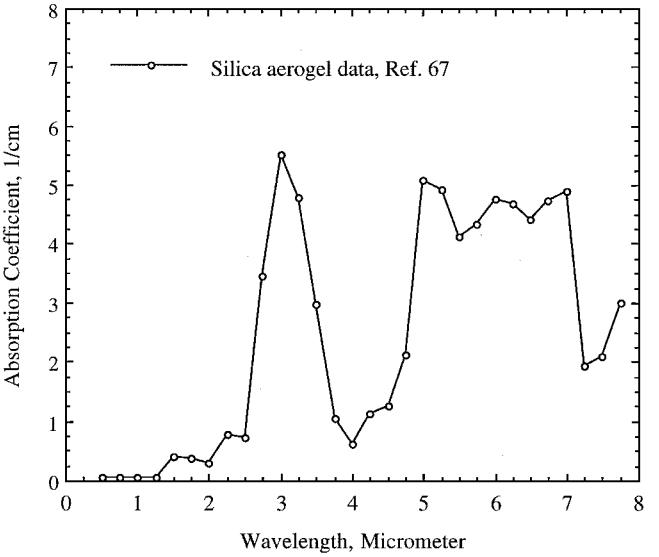

Fig. 11 Spectral absorption coefficient of silica aerogel calculated from measurement of normal transmittance.

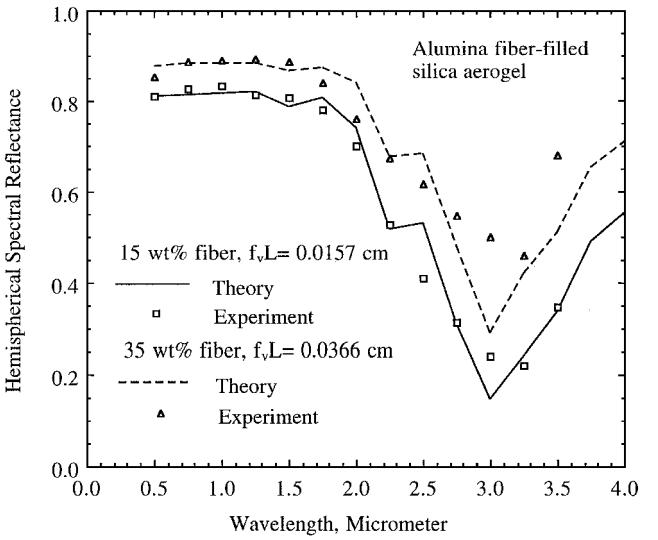

Fig. 12 Comparison of predicted and measured hemispherical spectral reflectance for alumina fiber-filled silica aerogels containing 15 and 35 wt% of fibers; specimen thickness L = 2.30 cm (Ref. 67).

fiber radiative properties. Normal spectral transmittances for equal f_vL values for type 1.7A and 1.7B fiber materials are shown in Fig. 9. Figure 10 shows the effect of f_vL on the normal spectral transmittance of two type 4.0B specimens of different thicknesses. The agreement between theory and measurement is very good in all cases, generally of the order of the experimental uncertainty. The transmittance for type 1.7B is slightly lower than that for type 1.7A (cf. Fig. 9) because of the narrower fiber size distribution, and both show lower transmittance than the larger fiber size type 4.0B material for equal values of f_vL.

Unbonded Fibers in an Absorbing Matrix

Fiber-loaded aerogels are materials that contain unbonded fibers in an absorbing matrix. The physical arrangement of fibers in the aerogel matrix for the specimens used in this study is shown by the SEM of Fig. 4. The fibers are randomly dispersed in the matrix with little evidence of fiber-to-fiber contact. The spectral absorption coefficient of the silica aerogel was determined from spectral normal transmittance measurements made on a sample of aerogel without fibers. The absorption coefficient data of silica aerogel, as seen in Fig. 11, show the high degree of transparency between the wavelength intervals of 0.5–2.5 and 3.5–4.5 μm. The real part of the complex refractive index (n) of the aerogel was estimated using the analysis of Caren[69] for finely divided, high-porosity medium of particles in the Rayleigh limit. The estimated value of n is 1.004–1.042 for wavelengths from 0.5 to 8 μm for aerogel densities of 80–160 kg/m^3, which correspond to those of the materials used in the present comparisons.

Spectral normal transmittance measurements were made on specimens of silica aerogels containing alumina and silica fibers. Manufacturer supplied data indicate that the average diameter of the alumina fibers is 3.17 μm, and the fiber composition is 97% alumina by weight with the balance silica. The size distribution of the silica fibers is given in Ref. 67, and the average diameter is 2.38 μm. The refractive index data reported in the preceding section for type B silica fiber material were used for these silica fibers, and data from Ref. 70 were used for the alumina fibers. The comparisons between predicted and measured hemispherical reflectances for two weight percentages of alumina fibers in silica aerogel are shown in Fig. 12. Similar comparisons for silica fibers in silica aerogel are shown in Fig. 13. The comparisons between theory and measurement of normal spectral transmittance for two weight percentages of silica fiber in silica aerogel are shown in Fig. 14. The agreement between theoretical prediction and measurement, both in magnitude and spectral

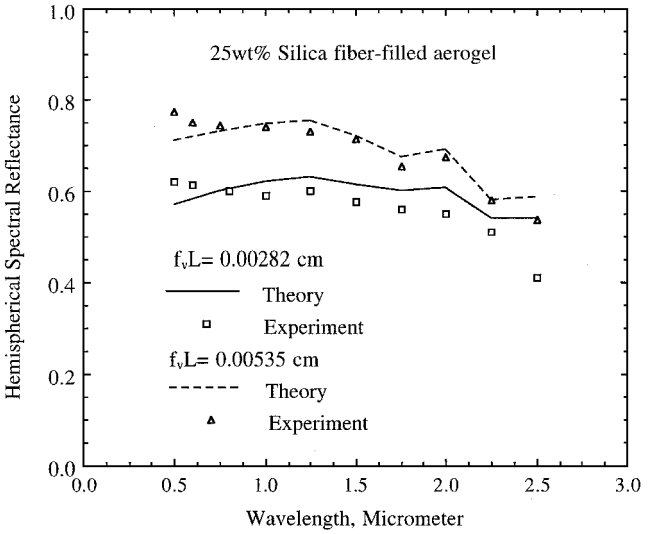

Fig. 13 Comparison of predicted and measured hemispherical spectral transmittance for two thicknesses of 25 wt% silica fiber-filled silica aerogel; f_v = 0.0141 (Ref. 67).

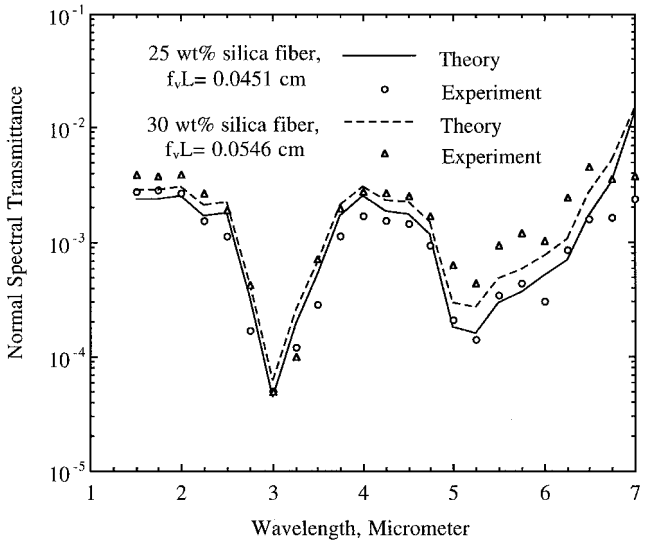

Fig. 14 Comparison of predicted and measured normal spectral transmittance for 0.32-cm-thick specimens of silica fiber-filled silica aerogels (bulk density = 125 kg/m^3) containing 25 and 30 wt% of fibers.[67]

variation, is very good in all instances. The strong decrease in reflectance between 2.5 and 3.5 μm for both fiber types is due to absorption by the aerogel (cf. Fig. 11). The maximum uncertainties in the experimental data are 0.01 μm in wavelength and 0.01 and 0.0003 for reflectance and transmittance, respectively.

Heat Transfer

Thermal conductivity data, measured in both vacuum and air over a wide temperature range for several types of insulation materials of various densities and thicknesses, are used for comparison with the radiation heat-transfer model. Because the experimental data for the fiber materials are measurements of the total heat flux, conduction caused by the solid and gas phases must be evaluated in each case. The prediction of the radiation conductivity of the fibrous media is given by Eqs. (21–24), solid- and gas-phase conductivities by Eqs. (25–33), and total heat transfer by Eqs. (35–39).

The experimental data consist of recent measurements on fiber-filled aerogels[52,53] and data reported in the literature for bonded[14] and unbonded[10,20] fiber insulations. The heat-transfer data were measured using several techniques. A guarded heat flow meter type of thermal conductivity apparatus described in Ref. 53 was used for measurements in air on materials that contain unbonded fibers in an absorbing matrix (fiber-filled aerogels). The test specimens, which were also used for transmittance and reflectance measurements, consisted of silica and silicon carbide fibers in a silica aerogel matrix. Thermal conductivity data for unbonded fiber insulations (loose fiber batts) were measured using two techniques, one a radial heat flow apparatus described in Ref. 10 and the other a guarded hot-plate thermal conductivity apparatus.[20] Thermal conductivity data for bonded fiber insulations (LI900 shuttle tile material) were obtained from measurements using a guarded hot-plate apparatus.[14] In the latter case the same test specimens were used for measurements of reflectance and transmittance[66] after completion of the heat-transfer measurements.

Bonded Fiber Materials in Air at Low Pressure

The bonded fiber test specimens used for the validation of the heat-transfer model are the type 1.7A, 1.7B, and 4.0B materials. Although the heat-transfer data were obtained under vacuum conditions,[14] heat conduction through the continuous matrix of bonded fiber arrays is not negligible compared to that by radiation. The geometric factor of Eq. (25) for each of the three fiber materials was determined from the thermal conductivity measured in vacuum at a pressure of <1 Pa and at a mean temperature of 110–120 K with a temperature gradient between boundaries of 50 K. Under these conditions the radiative heat flux is calculated to be less than 0.3 W/m^2 for the 2.54-cm-thick test specimens, which is less than 2% of the total heat flux. The calculations used the bulk density of each material and the thermal conductivity of fused silica evaluated at the mean temperature of the boundaries. The variation of the numerical value of F_s between the three materials was less than 1%.

By using a polynomial fit of the temperature variation of the thermal conductivity of silica[71] up to 1600 K and the average value of F_s obtained for the three materials, the temperature-dependent solid-phase thermal conductivity of the bonded fiber materials is

$$k_c(T) = \rho_s(8.07 \times 10^{-6} T^{\frac{1}{3}} + 4.80 \times 10^{-14} T^3) \qquad (45)$$

in units of W/m-K for bulk density given in kg/m^3. The relative magnitudes of the predicted radiation conductivity by Eq. (21) and solid-phase conductivity by Eq. (45) for type 1.7B and 4.0B materials are shown in Fig. 15. Corresponding results for the type 1.7A material, which has a smaller fiber volume fraction, are not shown in order to avoid cluttering the figure, as they are only slightly greater than those for type 1.7B. The solid-phase thermal conductivity is essentially the same for all three materials. There is, however, a large difference in the radiation conductivity between type 1.7B and 4.0B materials, which is caused by the difference in fiber diameter.

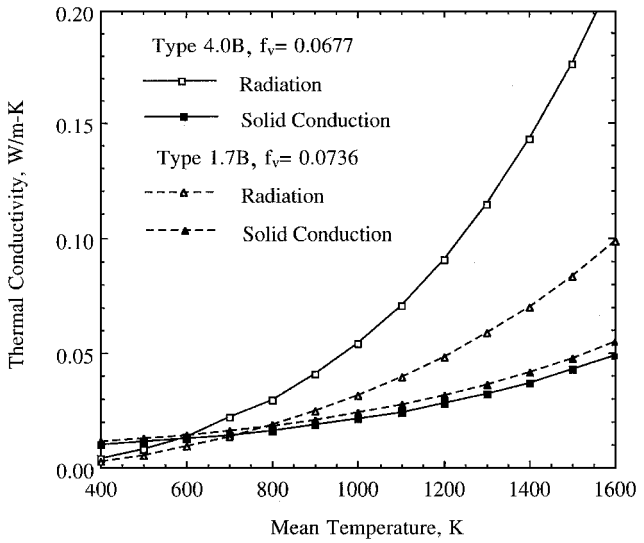

Fig. 15 Theoretical prediction of radiation and conduction thermal conductivities of type 1.7B and 4.0B materials.

Table 3 Comparison of thermal conductivity from Eqs. (38) and (39)

Temperature, K	Thermal conductivity × 100, W/m-K					
	Type 1.7A		Type 1.7B		Type 4.0B	
	Eq. (38)	Eq. (39)	Eq. (38)	Eq. (39)	Eq. (38)	Eq. (39)
500	1.851	1.846	2.032	2.029	1.691	1.686
700	3.144	3.139	3.619	3.618	2.785	2.778
900	4.991	4.984	6.088	6.091	4.301	4.289
1100	7.539	7.526	9.761	9.770	6.346	6.327
1300	10.97	10.95	15.03	15.05	9.059	9.031
1500	15.48	15.45	22.31	22.35	12.60	12.56

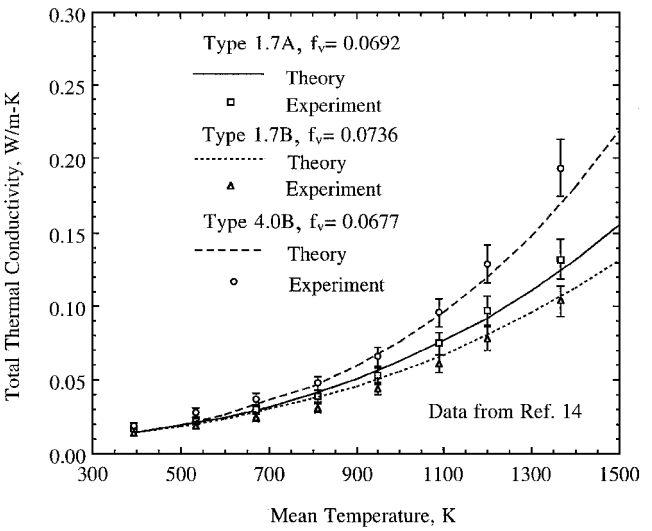

Fig. 16 Comparison of predicted and measured thermal conductivities in vacuum for type 1.7A, 1.7B, and 4.0B materials; specimen thickness L = 2.54 cm.

The maximum uncertainties in the predicted thermal conductivities caused by uncertainties in the fiber size and optical constants are for radiation, 20% at a temperature of 400 K, decreasing linearly to 6% at 900 K, and 4% at 1500 K; and for conduction, a constant uncertainty of 10% for temperatures from 400 to 1500 K.

Figure 16 shows the comparison between experimental data and theoretical predictions of the total thermal conductivity for the three types of bonded fiber materials. Type 4.0B material has the highest thermal conductivity and type 1.7B the lowest. Because the solid-phase conduction is comparable for the three materials, the different magnitudes are caused by the radiative conductivities as shown in Fig. 15. The maximum experimental uncertainties are 10% for thermal conductivity and 0.5% for temperature. The agreement between prediction and test data is within the experimental uncertainties at all temperatures. However, the data for type 4.0B indicate a trend of a slightly greater temperature dependence than is seen from the theoretical results. This discrepancy may be caused by a variation of spectral index of refraction with temperature. Although temperature-dependent values of the absorption index k from the literature for silica were used in the calculations, only ambient temperature data for the refractive index n of fused silica are available. Because fiber extinction is mainly by scattering at the shorter wavelengths, a small decrease in the refractive index at high temperature would substantially reduce the scattering efficiency and result in higher radiative heat transfer.

Table 3 shows the comparison of the total thermal conductivity based on the total heat flux calculated from Eq. (38) and the sum of the radiation and solid thermal conductivities. The difference between the results for the two methods is less than 0.5%. This is as expected for the optically thick media, and the optical thicknesses of all test specimens were greater than 25 for wavelengths between 0.5 and 25 μm.

Unbonded Fibers in Vacuum

Thermal conductivity data for two unbonded fiber materials that contain fibers randomly oriented in space are used for comparison with the present radiation heat-transfer model. In both cases the experimental data were measured under vacuum conditions at a pressure of less than 2 Pa. As the bulk densities are small, the solid-phase conduction caused by fiber-to-fiber contacts contributed to less than 2% of the total heat flux.

The first set of data used for comparison is that of Tong et al.[20] for a commercial low-density batt-type building insulation composed of glass fibers having a mean diameter of 6.9 μm and of a chemical composition similar to that of the soda-lime family of glasses. The reported bulk density was 8.4 kg/m^3, which corresponds to a fiber volume fraction of 3.3×10^{-3}. Measurements were made on three thicknesses of the insulation in vacuum at a pressure of less than 2 Pa using a guarded hot-plate apparatus with the boundary surfaces having a total hemispherical emittance of 0.95. The cold boundary temperature was fixed at 308 K, and the hot boundary temperatures were 363, 393, and 423 K. The estimated uncertainty of their measurements is given as 3%. The theoretical predictions of the present model were made using the fiber size distribution reported by Tong[72] and the recommended refractive index data[73] for a soda-lime type of glass. Figure 17 shows the comparison between the measured and predicted radiative heat fluxes. With the exception of a single data point for the 3.3 cm thickness specimen at a hot boundary temperature of 423 K, the theoretical prediction agrees with the experimental data to within 8%. This single value appears to be low when compared to the test data for the other thicknesses at the same hot boundary temperature. The original radiation models by Tong and Tien[19] produced poor agreement with their data, as is seen from Table 4, even when the apparent spectral extinction coefficients deduced from their transmittance measurements were used in their computation.

The second set of unbonded fiber data is from Pettyjohn[10] for a fused silica fiber insulation described as having a mean fiber diameter of 1.3 μm with no size distribution information given. Thermal conductivity data were presented for three bulk densities at mean temperatures between 400 and 800 K under vacuum conditions at a pressure of 1.3 Pa. The thermal conductivity measurements were made using a radial heat flow type of apparatus having a specimen thickness of 6 cm. Specimen bulk densities were 55, 98, and 149 kg/m^3. The solid conductivity due to the silica fiber matrix was estimated to be 2×10^{-4}, 3×10^{-4}, and 5×10^{-4} W/m-K for bulk densities of 55, 98, and 149 kg/m^3, respectively. These conductivities represent 0.5–1.5% of the total conductivities measured under vacuum conditions.

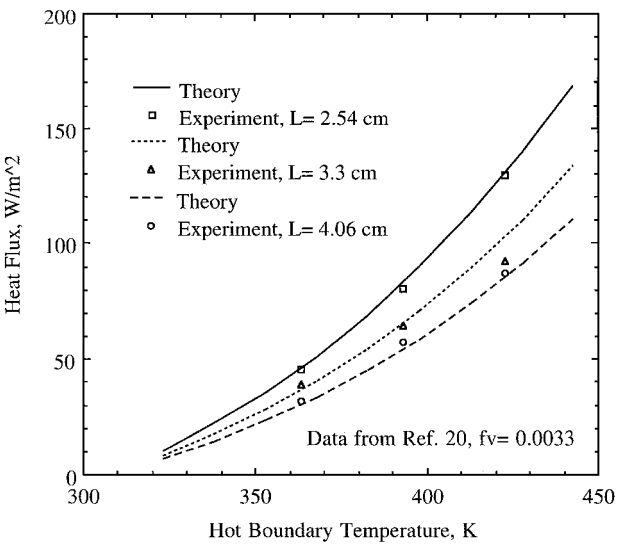

Fig. 17 Comparison of measured heat flux data from Ref. 20 with prediction using current theory for three thicknesses of glass fiber insulation with f_v = 0.0033 for the cold boundary at 308 K.

Table 4 Heat fluxes calculated by present model compared to Ref. 20 results

Hot side temperature, K	Heat flux, W/m^2			
	Present model	Experimental data[20]	Two-flux model[20]	LAS model[20]
	Insulation thickness = 2.54 cm			
363	45.3	45.8	27	33
393	82.4	80.2	49	59
423	130.0	129.2	75	90
	Insulation thickness = 3.30 cm			
363	35.8	38.7	21	26
393	65.0	64.9	38	46
423	102.7	92.6	62	71
	Insulation thickness = 4.06 cm			
363	29.6	31.9	18	21
393	53.7	57.4	32	38
423	84.8	87.2	49	60

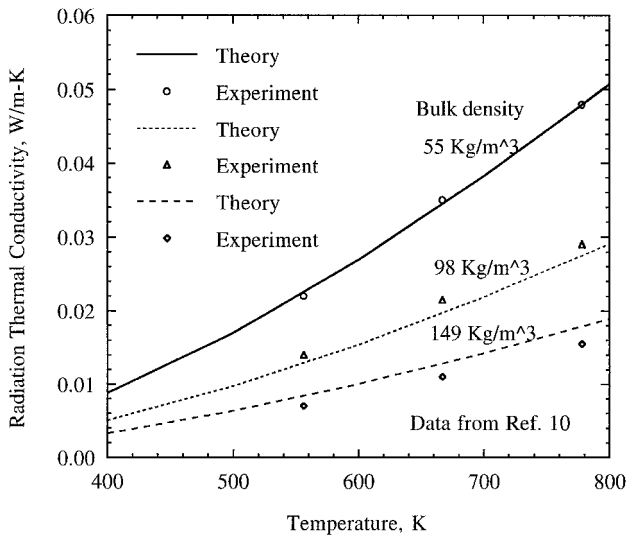

Fig. 18 Comparison of predicted and measured[14] thermal conductivities for three densities of unbonded silica fiber insulation in vacuum; specimen thickness L = 6 cm for all cases.

The comparison between theory and experiment is shown in Fig. 18 for the three insulation bulk densities. Theoretical predictions from the present model used the reported fiber density and fiber diameter, as well as the refractive index of fused silica.[68] Although the accuracy of the experimental data was not given in the reference,[10] we estimated the uncertainties to be 10% for thermal conductivity and 0.5% for temperature based on our experience with similar test apparatus. The corresponding maximum uncertainties in the prediction caused by uncertainties in optical constants and fiber size are the same as those for the bonded fiber analysis, 8–12%. The agreement between theory and experiment is generally very good and is within the aggregate of experimental and calculation uncertainties. The reason for the larger and nearly constant percentage-wise deviations seen for the highest density material may be caused by experimental errors associated with some guarding imbalance in the measurement of the smaller heat fluxes. Another potential reason is that some preferential orientation of the fibers resulted from the greater compaction in producing the higher density test specimen. Alignment of some fibers normal to the direction of heat would result in a larger extinction coefficient, thus resulting in lower radiation heat transfer than that for spatially randomly oriented fibers.

Unbonded Fibers in an Absorbing Matrix

Heat-transfer data for three silica fiber-filled silica aerogels of different densities and fiber volume fractions[53] are used for comparison with the model predictions. The fiber size distribution, given in Ref. 67, has an average diameter of 2.38 μm and a standard deviation of 1.2 μm. The fiber volume fractions of the three aerogel composites designated as 1, 2, and 3 are 0.017, 0.030, and 0.027, respectively. The respective bulk densities of these composites are 128, 146, and 198 kg/m^3, and the corresponding aerogel bulk densities are 91, 80, and 139 kg/m^3. Figure 19 shows the comparison of the calculated solid-phase thermal conductivities from Eq. (27) and experimental data over a limited temperature range for several silica aerogel densities densities of 96 and 220 kg/m^3. Also shown in the figure are predictions for two other aerogel densities. The good agreement between prediction and measurements validated the approach to calculate the solid-phase thermal conductivity for unloaded aerogels. The gas-phase thermal conductivities are calculated by utilizing Eq. (28) for air at atmospheric pressure filling the voids. The predictions are shown in Fig. 20 for two silica aerogel bulk densities and two values of macromolecular particle diameters of 2 and 5 nm used by Eq. (32) in the calculation of the pore diameter. These diameters represent the estimated bounds of the macromolecule particle size of the test specimens. The decrease in the gas-phase conductivity at higher temperatures is caused by the greater increase of the air mean free path with temperature than that of air thermal conductivity.

Comparisons of the measured total thermal conductivities with theoretical predictions based on Eqs. (21), (27), and (28) for the

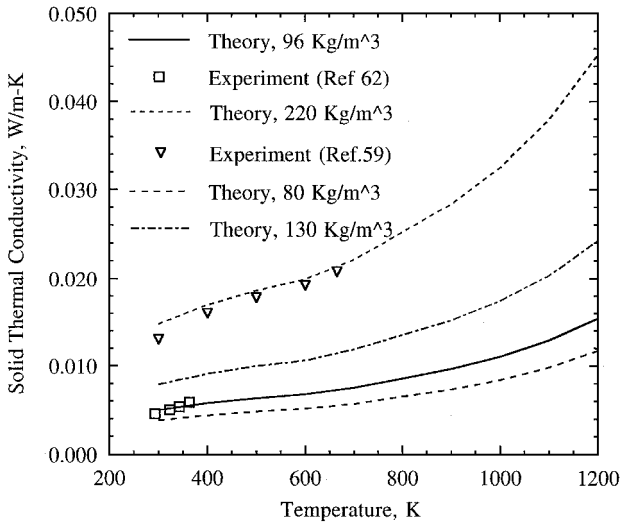

Fig. 19 Comparison of predicted and measured solid-phase thermal conductivities of silica aerogels at several bulk densities.

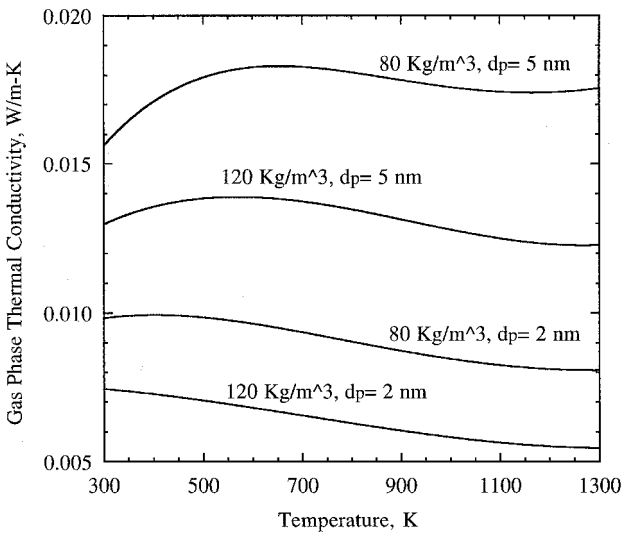

Fig. 20 Predicted gas-phase thermal conductivity of silica aerogel in air at atmospheric pressure for two aerogel bulk densities and two values of macromolecule diameter d_p.

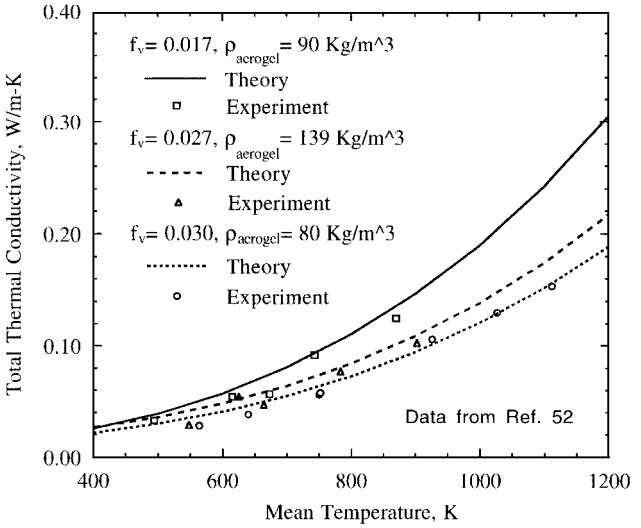

Fig. 21 Comparison of predicted and measured total thermal conductivities for three silica fiber-filled silica aerogel composites in air at atmospheric pressure.

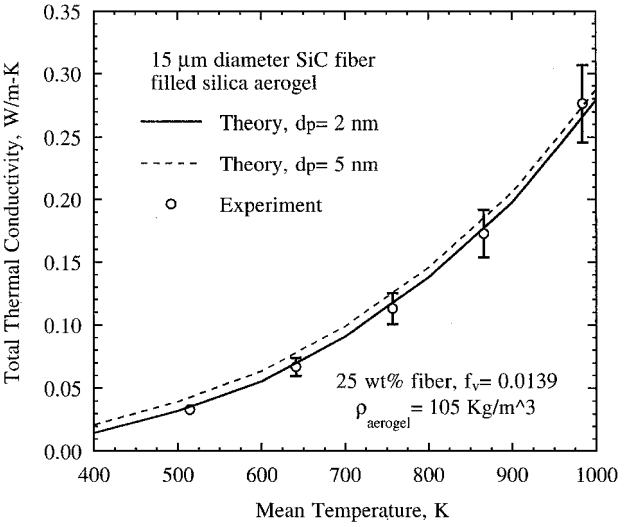

Fig. 22 Comparison of predicted and measured thermal conductivity of silicon carbide fiber-filled silica aerogel, in which fibers are predominantly oriented in planes normal to the heat flow direction.[52]

three aerogels are shown in Fig. 21. The maximum experimental uncertainties are 11% at 400 K increasing linearly to 13% at 1300 K for thermal conductivity and 0.5% for temperature. The estimated uncertainties in the theoretical total thermal conductivity are 15% at 400 K decreasing linearly to 10% at 1200 K. The agreement between theory and experiment is very good both in terms of the absolute value and in the temperature dependence. The theoretical values are generally within 10% of the measured data, and this deviation is well within the bounds of the rms error based on the sum of the experimental and theoretical uncertainties.

Oriented Fibers in an Absorbing Matrix

Thermal conductivity measurements of a silicon carbide (SiC) fiber-filled silica aerogel are used to test the validity of the radiation model for case of preferential fiber orientation.[52] This composite contains 15-μm-average-diameter, high-modulus silicon carbide fibers in a silica aerogel matrix. The fibers are drawn from an organic precursor so that the size distribution is very narrow with all fibers falling within the 13- to 17-μm-diam band. The fiber volume fraction is 0.0137, and the bulk density of aerogel is 105 kg/m^3. As determined by optical microscopy, the fibers are randomly oriented predominantly in planes normal to the direction of heat flow in the slab of test material. This fiber orientation is the result of settling of the large diameter and very stiff fibers during the aerogel gelation process. Figure 22 shows the comparison between experimental data and theoretical predictions based on Eqs. (21), (27), and (28), assuming that all of the fibers are randomly oriented in planes parallel to the boundaries. Calculation of the gas-phase thermal conductivity again assumed that the diameters of the macromolecules that make up the structure of the aerogel lie between 2 and 5 nm. These two sizes are considered to be representative of the bounds of uncertainty in this silica aerogel structural characterization. The agreement between theory and measurement is well within the limits of experimental uncertainty shown on the data points. The maximum uncertainty in the theoretical values is 12% at 400 K, decreasing to 9% at 1000 K.

The influence of fiber orientation on radiative thermal conductivity is illustrated by the theoretical calculations shown in Fig. 23 for SiC fibers in silica aerogel. The fiber size and volume fraction, as well as the composite bulk density, are identical to those of Fig. 22. Fibers randomly oriented in planes normal to the heat flow direction result in significantly lower radiative thermal conductivities than those for fibers randomly oriented in space. The intermediate curve shows the effect of mixing random in-space with random in-plane fibers in equal proportions. Although fibers oriented in planes give the lowest thermal conductivity, it can be desirable to incorporate some fraction of fibers in a spatially random orientation to increase the shear strength of the material.

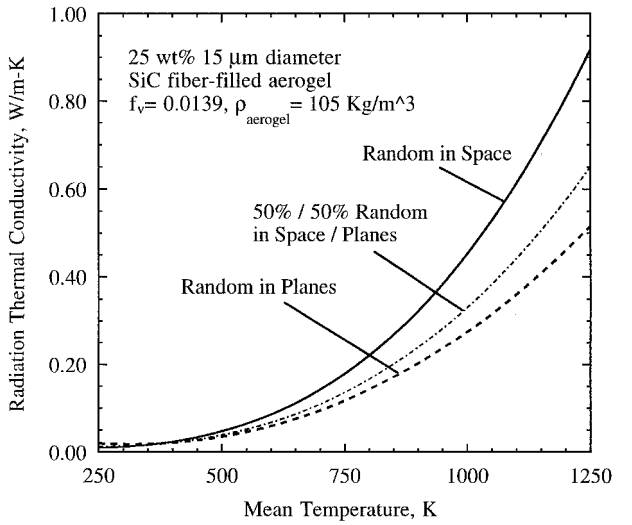

Fig. 23 Effect of fiber orientation on the radiative thermal conductivity of silicon carbide fiber-filled silica aerogel in air at atmospheric pressure.[54]

Comparison of Data with Existing Radiation Models

Comparisons of the experimental data and the predicted total thermal conductivities using the existing two-flux and diffusion models are shown in Figs. 24 and 25 for the bonded fiber insulations of types 1.7B and 4.0B. The solid-phase thermal conductivities based on Eq. (25) are added to the radiation conductivity calculated using the conventional two-flux and diffusion models. The boundary surface emittances for the calculations are assumed to be gray and equal to 0.8, which corresponds to the experimental conditions. The two-flux models refer to those by both Tong and Tien[19] and Lee.[35] As the results from both models differ by less than 10%, the two-flux predictions shown in the figures are representative of both models. The results designated as Rosseland mean refer to the diffusion model in which the fiber extinction coefficient is used in Eq. (21) in place of the absorption coefficient. The poor agreement of the conventional two-flux and Rosseland mean model results with experimental data reveals the deficiency of these modeling methodologies for radiative transfer in fibrous media.

Similar results are seen from the comparison between the heat flux predictions using the present theoretical model with those from

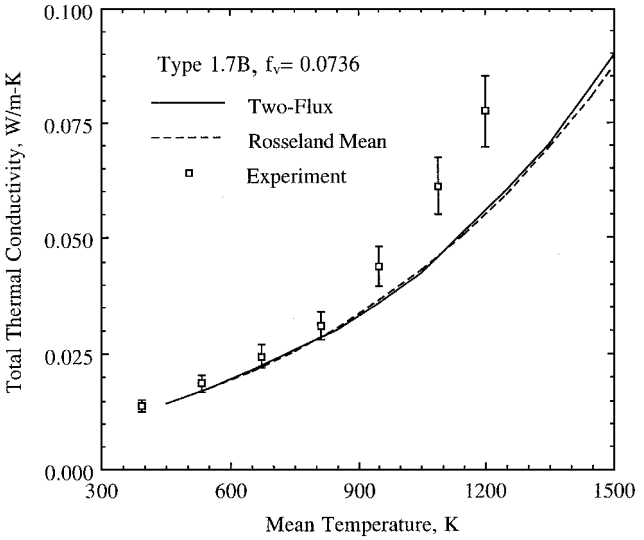

Fig. 24 Comparison of measured thermal conductivity for type 1.7B material in vacuum with predictions based on the conventional two-flux and Rosseland mean models for the radiative thermal conductivity.

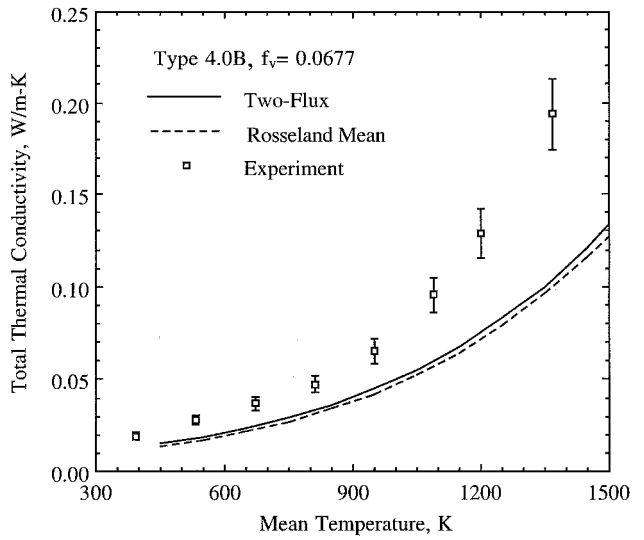

Fig. 25 Comparison of measured thermal conductivity for type 4.0B material in vacuum with predictions based on the conventional two-flux and Rosseland mean models for the radiative thermal conductivity.

Tong et al.[20] for the two-flux and linear anisotropic scattering (LAS) models. These results together with their experimental data are presented in Table 4. The two-flux model predictions fall 40–45% below the experimental values, and the LAS model results lie 30–35% below the experimental values. The predictions from the present study are within 8% of the experimental values.

Conclusion

The validity of the theoretical formulations presented in this paper for the radiative properties and radiation heat transfer in high-porosity fibrous media is affirmed by the close agreement of predictions with a comprehensive base of experimental data. The materials used for tests were well-characterized, and the experimental methods and their accuracies defined. The data included both measurements reported in the literature and those recently obtained for some special fiber materials. The radiation model uses only deterministic material properties and does not require any adjustable parameters for matching with experimental results. Comparisons of experimental data of spectral reflectance and transmittance with theoretical predictions demonstrate the high degree of accuracy of the formalisms for radiative properties. The good agreement underlines the importance of the rigorous accounting of fiber orientation in the theoretical formulation.

The radiation heat-transfer model is based on the diffusion approximation using a modified Rosseland mean coefficient that corrects for the effect of scattering by fibers and absorption of the matrix medium. The radiation model produced excellent agreement with experimental heat-transfer data for a variety of fiber materials that contain bonded fibers, unbonded fibers, with and without an absorbing matrix, and fibers randomly or preferentially oriented. The success of the model is due to the rigorous formulations of the fiber radiative properties and the modified extinction coefficient that include the effect of fiber orientation. The absence of rigorous accounting of the effect of fiber orientation in the other conventional two-flux and diffusion models resulted in their poor agreement with measured data.

References

[1]Lee, S. C., "Dependent Versus Independent Scattering in Fibrous Composites Containing Parallel Fibers," *Journal of Thermophysics and Heat Transfer*, Vol. 8, No. 4, 1994, pp. 641–646.

[2]Lee, S. C., and Cunnington, G. R., "Theoretical Models for Radiative Transfer in Fibrous Media," *Annual Review in Heat Transfer*, edited by C. L. Tien, Vol. 9, Begell House, New York, 1998, pp. 159–218.

[3]Kagner, M. G., *Thermal Insulation in Cryogenic Engineering*, Catalog No. 2200, Israel Program for Scientific Translations, Ltd., Jerusalem, 1969, Chaps. 1, 4, and 5.

[4]Verschoor, J. D., and Greebler, P., "Heat Transfer by Gas Conduction and Radiation in Fibrous Insulation," *Transactions of the American Society of Mechanical Engineers*, Vol. 74, No. 6, 1952, pp. 961–968.

[5]Van der Held, E. F. M., "The Contribution of Radiation to the Conduction of Heat," *Applied Scientific Research*, Sec. A, Vol. 3, 1952, pp. 237–249.

[6]Van der Held, E. F. M., "The Contribution of Radiation to the Conduction of Heat, II. Boundary Conditions," *Applied Scientific Research*, Sec. A, Vol. 4, 1953, pp. 77–99.

[7]Christiansen, R. M., and Hollingsworth, M., "The Performance of Glass Fiber Insulation Under High Vacuum," *Advances in Cryogenic Engineering*, Vol. 4, 1960, pp. 141–153.

[8]Strong, H. M., Bundy, F. P., and Bovenkerk, H. P., "Flat Panel Vacuum Thermal Insulation," *Journal of Applied Physics*, Vol. 31, No. 1, 1960, pp. 39–50.

[9]Hager, N. E., Jr., and Steere, R. C., "Radiant Heat Transfer in Fibrous Thermal Insulation," *Journal of Applied Physics*, Vol. 38, No. 10, 1967, pp. 4663–4668.

[10]Pettyjohn, R. R., "Thermal Conductivity Measurements on a Fibrous Insulation Material," *Proceedings of the Seventh Conference on Thermal Conductivity*, NBS Special Publication 302, edited by D. R. Flynn and B. A. Leavy Jr., U.S. Government Printing Office, Washington, DC, 1968, pp. 729–736.

[11]Bankvall, C. G., "Heat Transfer in Fibrous Materials," *Journal of Testing and Evaluation*, Vol. 1, No. 3, 1973, pp. 235–243.

[12]Linford, R. M. F., Schmitt, R. J., and Hughes, T. A., "Radiative Contribution to the Thermal Conductivity of Fibrous Insulations," *Heat Transmission Measurements in Thermal Insulations*, Special Publication 544, American Society for Testing and Materials, Philadelphia, 1974, pp. 68–84.

[13]Davis, L. B., Jr., and Birkebak, R. C., "On the Transfer of Energy in Layers of Fur," *Biophysics Journal*, Vol. 14, 1974, pp. 249–268.

[14]Banas, R. P., and Cunnington, G. R., "Determination of the Effective Thermal Conductivity of the Space Shuttle Orbiter's Reusable Surface Insulation (RSI)," AIAA Paper 74-730, July 1974.

[15]Pelanne, C. M., "Heat Flow Principles in Thermal Insulations," *Journal of Thermal Insulation*, Vol. 4, No. 1, 1980, pp. 27–44.

[16]Larkin, B. K., and Churchill, S. W., "Heat Transfer by Radiation Through Porous Insulations," *Journal of the American Institute of Chemical Engineers*, Vol. 5, No. 4, 1959, pp. 467–474.

[17]Hottel, H. C., and Sarofim, A. F., *Radiative Transfer*, McGraw-Hill, New York, 1967, pp. 378–436.

[18]Tong, T. W., and Tien, C. L., "Analytical Models for Thermal Radiation in Fibrous Media," *Journal of Thermal Insulation*, Vol. 4, 1980, pp. 27–44.

[19]Tong, T. W., and Tien, C. L., "Radiative Transfer in Fibrous Insulations-Parts 1: Analytical Study," *Journal of Heat Transfer*, Vol. 105, No. 1, 1983, pp. 70–75.

[20]Tong, T. W., Yang, Q. S., and Tien, C. L., "Radiative Transfer in Fibrous Insulations-Part 2: Experimental Study," *Journal of Heat Transfer*, Vol. 105, No. 1, 1983, pp. 76–81.

[21]Houston, R. L., and Korpela, S. A., "Heat Transfer Through Fiberglass Insulation," *Proceedings of the 7th International Heat Transfer Conference*, Vol. 2, Hemisphere, Washington, DC, 1982, pp. 499–504.

[22]Tong, T. W., Swathi, P. S., and Cunnington, G. R., "Reduction of Radiative Heat Transfer in Thermal Insulations by Use of Dielectric Coated Fibers," *International Communications in Heat and Mass Transfer*, Vol. 16, No. 6, 1989, pp. 851–860.

[23]Mathes, R., Blumenberg, J., and Keller, K., "Radiative Heat Transfer in Insulations with Random Fiber Orientation," *International Journal of Heat and Mass Transfer*, Vol. 33, No. 4, 1990, pp. 767–770.

[24]Stark, C., and Fricke, J., "Improved Heat-Transfer Models for Fibrous Insulations," *International Journal of Heat and Mass Transfer*, Vol. 36, No. 3, 1993, pp. 617–625.

[25]Dombrovsky, L. A., "Calculation of Spectral Radiative Properties of Quartz Fibrous Insulation in the Infrared," *Proceedings of the 10th International Heat Transfer Conference*, Vol. 2, edited by G. F. Hewitt, Taylor and Francis, Bristol, PA, 1994, pp. 25–30.

[26]Dombrovsky, L. A., "Quartz-Fiber Thermal Insulation: Infrared Radiative Properties and Calculation of Radiative-Conductive Heat Transfer," *Journal of Heat Transfer*, Vol. 118, No. 2, 1996, pp. 408–414.

[27]Cohen, L. D., Haracz, R. D., Cohen, A., and Acquista, C., "Scattering of Light from Arbitrarily Oriented Finite Cylinders," *Applied Optics*, Vol. 22, No. 5, 1983, pp. 742–748.

[28]Matthews, L. K., Viskanta, R., and Incropera, F. P., "Development of Inverse Methods for Determining Thermophysical and Radiative Properties of High Temperature Fibrous Materials," *International Journal of Heat and Mass Transfer*, Vol. 27, No. 3, 1984, pp. 487–495.

[29]Yeh, H. Y., and Roux, J. A., "Spectral Radiative Properties of Fiberglass Insulations," *Journal of Thermophysics and Heat Transfer*, Vol. 2, No. 1, 1989, pp. 78–81.

[30]Kamiuto, K., Sato, M., and Iwamoto, M., "Determination of the Radiative Properties of High-Porosity Materials by Use of the Emerging-Intensity Fitting Method," *Journal of Quantative Spectroscopy and Radiative Transfer*, Vol. 42, No. 4, 1989, pp. 477–482.

[31]Kurosaki, Y., Yamada, J., and Take-Uchi, M., "Estimation of the Radiative Properties of Fibrous Media Taking Account of Fiber Orientation," *Proceedings of the ASME/JSME Thermal Engineering Conference*, Vol. 4, 1991, pp. 11–18.

[32]Petrov, V. A., "Inverse Radiation Problems in Scattering Semitransparent Materials Based on the Radiation Diffusion Approximation," *Proceedings of the 13th European Conference on Thermophysical Properties*, 1993.

[33]Kuhn, J., Korder, S., Arduini-Schuster, M. C., Gobel, G., and Fricke, J., "Infrared-Optical Properties of Insulating Powders," *Proceedings of the 13th European Conference on Thermophysical Properties*, 1993.

[34]Nicolau, V. P., Raynard, M., and Sacadura, J. F., "Spectral Radiative Properties Identification of Fiber Insulating Materials," *International Journal of Heat and Mass Transfer*, Vol. 37, Supplement 1, 1994, pp. 311–324.

[35]Lee, S. C., "Radiative Transfer Through a Fibrous Medium: Allowance for Fiber Orientation," *Journal of Quantative Spectroscopy and Radiative Transfer*, Vol. 36, No. 3, 1986, pp. 253–263.

[36]Lee, S. C., "Radiation Heat Transfer Model for Fibers Oriented Parallel to Diffuse Boundaries," *Journal of Thermophysics and Heat Transfer*, Vol. 2, No. 4, 1988, pp. 303–308.

[37]Lee, S. C., "Effect of Fiber Orientation on Thermal Radiation in Fibrous Media," *International Journal of Heat and Mass Transfer*, Vol. 32, No. 2, 1989, pp. 311–319.

[38]Lee, S. C., "Scattering Phase Function for Fibrous Media," *International Journal of Heat and Mass Transfer*, Vol. 33, No. 10, 1990, pp. 2183–2190.

[39]Boulet, P., Jeandel, G., and Morlot, G., "Model of Radiative Transfer in Fibrous Media-Matrix Method," *International Journal of Heat and Mass Transfer*, Vol. 36, No. 2, 1993, pp. 4287–4297.

[40]Jeandel, G., Boulet, P., and Morlot, G., "Radiative Transfer Through a Medium of Silica Fibers Oriented in Parallel Planes," *International Journal of Heat and Mass Transfer*, Vol. 36, No. 4, 1993, pp. 531–536.

[41]Boulet, P., Jeandel, G., Morlot, G., Silberstein, A., and Dedianous, P., "Study of the Radiative Behavior of Several Fiberglass Materials," *Thermal Conductivity 22*, edited by T. W. Tong, Technomic, Lancaster, PA, 1994, pp. 749–759.

[42]Siegel, R., and Howell, J. R., *Thermal Radiation Heat Transfer*, 3rd ed., McGraw–Hill, New York, 1992, Chap. 18.

[43]Roux, J. A., and Smith, A. M., "Combined Conduction and Radiation Heat Transfer in a Absorbing and Scattering Medium," American Inst. of Chemical Engineers/American Society of Mechanical Engineers, Paper 77-HT-50, Aug. 1977.

[44]Matthews, L. K., Viscanta, R., and Incropera, F. P., "Combined Conduction and Radiation Heat Transfer in Porous Materials Heated by Intense Solar Radiation," *Journal of Solar Energy*, Vol. 107, 1985, pp. 29–34.

[45]Keller, K., and Blumenberg, J., "High Temperature Airborne Fibre Insulations Heat Transfer," *Proceedings of the Ninth International Heat Transfer Conference*, Vol. 5, edited by G. Hetsroni, Hemisphere, 1990, pp. 479–484.

[46]Petrov, V. A., "Combined Radiation and Conduction Heat Transfer in High Temperature Fibre Thermal Insulation," *International Journal of Heat and Mass Transfer*, Vol. 40. No. 9, 1997, pp. 2241–2247.

[47]Daryabeigi, K., "Analysis and Testing of High Temperature Fibrous Insulation for Reusable Launch Vehicles," AIAA Paper 99-1044, Jan. 1999.

[48]Lind, A. C., and Greenberg, J. M., "Electromagnetic Scattering for Obliquely Oriented Cylinders," *Journal of Applied Physics*, Vol. 37, No. 8, 1966, pp. 3195–3203.

[49]van de Hulst, H. C., *Light Scattering by Small Particles*, Dover, New York, 1981, Chap. 15.

[50]Kerker, M. C., *The Scattering of Light and Other Electromagnetic Radiation*, Academic, New York, 1969, Chap. 6.

[51]Barabas, M., "Scattering of a Plane Wave by a Radially Stratified Tilted Cylinder," *Journal of the Optical Society of America A*, Vol. 4, No. 12, 1987, pp. 2240–2248.

[52]Lee, S. C., and Cunnington, G. R., "Fiber Orientation Effect on Radiative Heat Transfer Through Fiber Composites," AIAA Paper 98-2840, June 1998.

[53]Cunnington, G. R., Lee, S. C., and White, S. M., "Radiation Heat Transfer in Fiber-Filled Silica Aerogel: Comparison of Theory with Experiment," AIAA Paper 97-3884, Aug. 1997.

[54]Lee, S. C., and Cunnington, G. R., "Heat Transfer in Fibrous Insulations: Comparison of Theory and Experiment," *Journal of Thermophysics and Heat Transfer*, Vol. 12, No. 3, 1998, pp. 297–303.

[55]Bejan, A., *Convective Heat Transfer*, Wiley, New York, 1984, pp. 343–416.

[56]Kistler, S. S., "Coherent Expanded Aerogels and Jellies," *Nature*, Vol. 127, 1931, p. 741.

[57]Hubruesh, L. W., and Pekala, R. W., "Thermal Properties of Organic and Inorganic Aerogels," Lawrence Livermore National Lab., Rept. UCRL-JC-111333, Livermore, CA, April 1993.

[58]Caps, R., and Fricke, J., "Infrared Radiation Heat Transfer in Highly Transparent Silica Aerogel," *Solar Energy*, Vol. 36, 1986, pp. 361–365.

[59]Fricke, J., Lu, X., Wang, P., Buttner, D., and Heinemann, U., "Optimization of Monolithic Silica Aerogel Insulants," *International Journal of Heat and Mass Transfer*, Vol. 35, No. 9, 1992, pp. 2305–2309.

[60]Nilsson, O., Bock, V., Caps, R., and Fricke, J., "High Temperature Thermal Properties of Carbon Aerogels," *Thermal Conductivity 22*, edited by T. W. Tong, Technomic, Lancaster, PA, 1994, pp. 878–887.

[61]Zeng, S. Q., Hunt, A. J., and Greif, R., "Geometric Structure and Thermal Conductivity of Porous Medium Silica Aerogel," *Journal of Heat Transfer*, Vol. 117, No. 4, 1995, pp. 1055–1058.

[62]Zeng, S. Q., Stevens, P. C., Hunt, A. J., Grief, R., and Lee, D., "Thin-Film-Heater Thermal Conductivity Apparatus and Measurement of Thermal Conductivity of Silica Aerogel," *International Journal of Heat and Mass Transfer*, Vol. 39, No. 11, 1996, pp. 2311–2317.

[63]Heinemann, U., Caps, R., and Fricke, J., "Radiation-Conduction Interaction: an Investigation of Silica Aerogels," *International Journal of Heat and Mass Transfer*, Vol. 39, No. 11, 1996, pp. 2115–2130.

[64]Keller, K., Blumenberg, J., and Tomsik, J., "Fibre Orientation and the Conduction of Heat by a Gas Enclosed in Ceramic Layers," *ZFW*, Vol. 12, 1988, pp. 258–260.

[65]Brewster, M. Q., *Thermal Radiative Transfer and Properties*, Wiley, New York, 1992, Chap. 12.

[66]Cunnington, G. R., and Lee, S. C., "Radiative Properties of Fibrous Thermal Insulations: Theory Versus Experiment," *Journal of Thermophysics and Heat Transfer*, Vol. 10, No. 3, 1996, pp. 460–466.

[67]Cunnington, G. R., Lee, S. C., and White, S. M., "Radiative Properties of Fiber-Reinforced Aerogel: Theory Versus Experiment," *Journal of Thermophysics and Heat Transfer*, Vol. 12, No. 1, 1998, pp. 17–22.

[68]Palik, E. D., *Handbook of Optical Constants of Solids*, Academic, Orlando, FL, 1985.

[69]Caren, R. P., "Radiation Heat Transfer from a Metal to a Finely Divided Particulate Medium," *Journal of Heat Transfer*, Vol. 93, No. 1, 1969, pp. 154–156.

[70]Malitson, I. H., Murphy, F. V., and Rodney, W. S., "Refractive Index of Synthetic Sapphire," *Journal of the Optical Society of America*, Vol. 48, No. 1, 1958, pp. 72–78.

[71]Incropera, F. P., and DeWitt, D. P., *Fundamentals of Heat Transfer*, 1st ed., Wiley, New York, 1981, Appendix A.

[72]Tong, T. W., "Thermal Radiation in Fibrous Insulations," Ph.D. Dissertation, Dept. of Mechanical Engineering, Univ. of California, Berkeley, CA, Oct. 1980.

[73]Hsieh, C. K., and Su, K. C., "Thermal Radiative Properties of Glass from 0.32 μm to 20.66 μm," *Solar Energy*, Vol. 22, 1978, pp. 37–43.